POLITECNICO DI TORINO

Master's Degree in Nuclear Engineering

Benchmark of the OpenSC^2 model in transients with significant current redistribution in superconducting cables for nuclear fusion.

Supervisors

Prof. Laura SAVOLDI

Dr. Daniele PLACIDO

Candidate

Alessandro MORTARA

July 2024

Abstract

Superconductivity is a critical enabling technology for magnetic confinement nuclear fusion. Different types of cables are under study in this field, with much effort in the scientific community focused on the use of high-temperature superconducting (HTS) cables, which enable the generation of more powerful magnetic fields. Numerous designs have been proposed and studied using various modeling software to predict the behavior of these cables under operational conditions. For LTS cables, various software programs (such as 4C, THEA, and VENECIA) can model both the electrical and thermohydraulic profiles. However, they are not recommended for the modeling of HTS cables for which the H4C code was introduced some years ago.

To address this need, OpenSC^2 was developed by the MAHTEP group at Politecnico di Torino. This open-source program facilitates multi-physics analysis for both LTS and HTS cables. The thermal-hydraulic model available in OpenSC^2 has already undergone a preliminary phase of verification and validation. The modeling capability of OpenSC^2 was improved by the possibility of coupling the thermal-hydraulic model to a lumped electric model based on a network of resistances, inductances and conductances, which is described in this thesis.

The objective of this work is to benchmark the coupling between the thermal-hydraulic and the electric models in OpenSC^2 against the results obtained with the H4C tool for a quench study of the 132 m long ENEA HTS cable. It carries a nominal current of 32.1 kA and is placed in a magnetic field of 17 T. Cooling is achieved using ~5 g/s of supercritical helium at 4.5 K and 0.6 MPa, allowing it to be introduced downstream of the same cryostat as the LTS cable, but with higher temperature margins in case of a tape quench. The quench of the cable is induced with a heat pulse 0.1-s-long of 150 J in 10 cm of the cable. After 0.25 s from the quench detection, the current is dumped according to an exponential law. Temperature peaks as well as current time evolution are compared to the outcomes of the H4C tool, based on the discharge rate of the current and the delay time in which this occurs.

To achieve this goal, it was necessary to suitably discretize the cable in sub-components; by exploiting the symmetry conditions present in the case study, it was found that 1/12 of the total geometry was representative of the cable. The choice of materials used to model the different sub-components was as accurate as possible, considering the real composition of the ENEA cable. However, assumptions are always necessary to simplify the analysis.

Finally, the quality of the results is guaranteed by space and time convergence analysis. Overall, the outcome of this analysis has shown that, duly considered the difference between the two software, OpenSC^2 achieves the same results predicted with 4C within a 13% accuracy.

Therefore, for this test case, it can be claimed that the coupling of the thermal-hydraulic and of the electric model in OpenSC^2 is consistent: during the transient as the electric resistance of the superconductor increases, the current is progressively redistributed on the stabilizer according to their electrical properties becoming the main driver for the thermal-hydraulic problem.

Outline

List of symbols

Scalar Quantities		
Quantity	Symbol	Unit SI
Voltage	V	V
Electric resistance	R	Ω
Electric current	I	A
Electric potential	φ	V
Inductance	L	H
Electric conductance	G	S
Time	t	s
Electrical resistivity	ρ_{el}	Ω m
Cross section	A	m^2
Reference electric field for the power law	E_0	V / m
Current density	J	A /m^2
Critical current density	J_c	A /m^2
Power law exponent	n	-
Conductor length	l	m
Linear heat source	Q	W / m
Density	ρ	kg / m^3
Velocity	v	m/s
Pressure	p	Pa
Specific energy	e	J / kg
Speed of sound	c	m / s
Specific heat at constant volume	c_v	J / (kg K)
Specific heat at constant pressure	c_p	J / (kg K)
Gruneisen parameter	Φ	-
Specific enthalpy	w	J / kg
Mass source term	Λ_ρ	kg / (m^3 s)
Momentum source term	Λ_v	J / m^4
Energy source term	Λ_e	W / m^3
Temperature	T	K

Quantity	Symbol	Unit
Thermal conductivity	k	W / (m K)
Thermal conductance	h_c	W / (m^2 K)
Contact perimeter	P	m
Difference	Δ	-
Partial derivative operation	∂	-
Spatial coordinate	x	m

Matrices and Vectors

Quantity	Symbol
Incidence matrix	$\boldsymbol{A_e}$
Matrix of the electric resistances	$\boldsymbol{R}$
Transpose incidence matrix	$\boldsymbol{A_e}^T$
Vector of currents	$\boldsymbol{I}$
Vector of electric potential	$\boldsymbol{\varphi}$
Matrix of the electric inductances	$\boldsymbol{L}$
Matrix of the electric conductances	$\boldsymbol{G}$
Vector of source currents	$\boldsymbol{I_S}$
Not null vector constituting the diagonal of the mass matrix	$\mathcal{M}$
Not null vector constituting the diagonal of the advection matrix	$\mathcal{A}$
Not null vector constituting the diagonal of the conductive matrix	$\mathcal{K}$
Not null vector constituting the diagonal of the source term matrix	$\mathcal{S}$
Vector of the unknowns	$\boldsymbol{u}$
Vector of the source terms	$\boldsymbol{s}$

1 Introduction

Superconductivity has a history of just over a hundred years [1], but since its accidental discovery [2], it has made tremendous progress. With the increasing understanding of the properties of superconducting materials (SC), many branches of application for this technology are being studied. These include SC magnets for nuclear fusion and electric generators, power transmission, energy storage devices, particle accelerators, levitated vehicle transportation, rotating machinery, fault current limiters, magnetic separators and magnetic resonance images.

This work can be classified in the field of superconducting magnets for magnetic confinement nuclear fusion, so what follows is an overview of why superconductivity can be exploited to build magnets used in nuclear fusion reactors (Section 1.1) and of the plethora of SC cables used to wind those magnets (Section 1.2). Being this thesis focused on numerical modeling, Section 1.3 discussed the state-of-art software available for modeling SC cables; finally in Section 1.4 the main objectives and the structure of the thesis is presented.

1.1 Nuclear Fusion and Superconductivity

Nuclear fusion for electricity production represents one of the most promising frontiers in the search for clean and sustainable energy sources [3]. Unlike nuclear fission, which splits heavy nuclei into lighter nuclei releasing energy, nuclear fusion occurs when light nuclei, such as those of hydrogen, combine to form a heavier nucleus, releasing enormous amounts of energy (Figure 1.1 – 1).
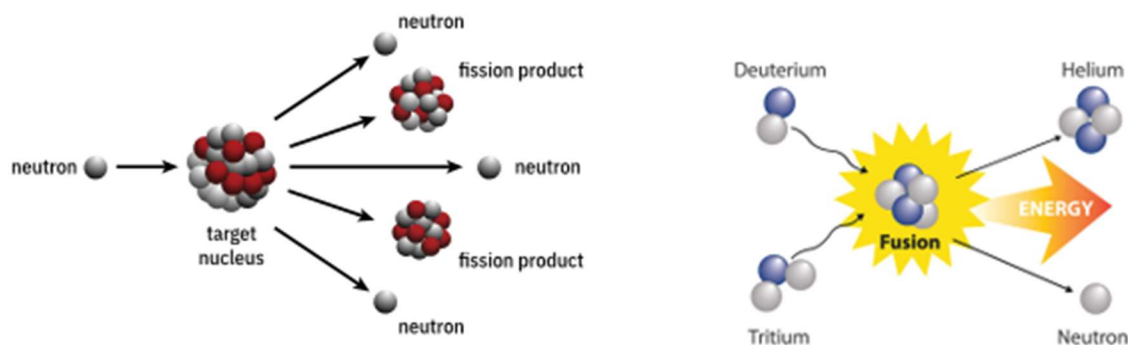

Figure 1.1 - 1: On the left, the diagram of a nuclear fission reaction. On the right, the diagram of a nuclear fusion reaction.

There are two main methods to achieve the conditions necessary for fusion: inertial confinement and magnetic confinement

Inertial confinement relies on the use of powerful energy pulses to compress a small pellet of fusion fuel until the conditions necessary for fusion are achieved [4]. This technology utilizes physics that does not involve superconductivity, and therefore will not be discussed further in this text.

Magnetic confinement uses powerful magnetic fields to keep the plasma (an ionized gas composed of nuclei and electrons) hot, stable, and confined. Among the devices used for magnetic confinement are the tokamak [5] and the stellarator [6] (Figure 1.1 – 2).
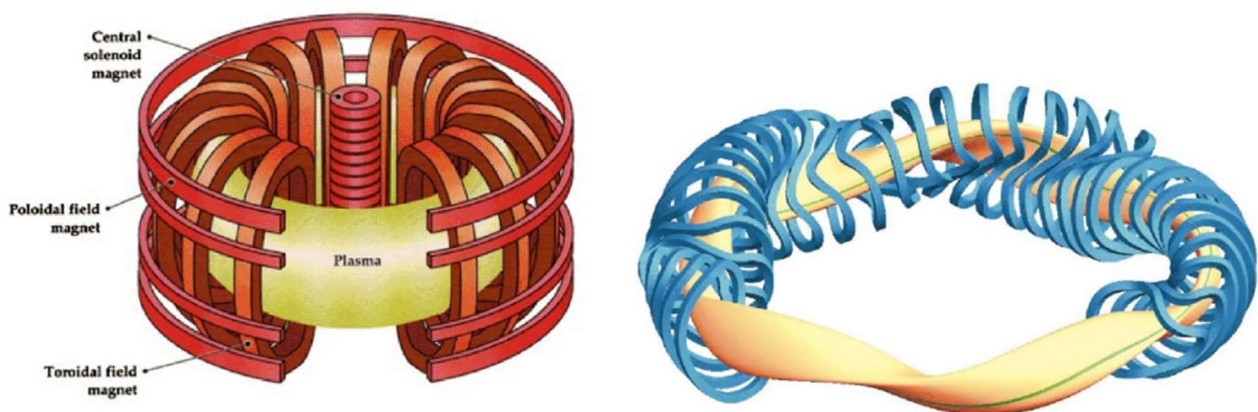

Figure 1.1 - 2: Diagrams of the coil systems used in fusion reactors bases on magnetic confinement and associated plasma shape. Left: Tokamak. Right: Stellarator. Image adapted from [7].

Research on fusion has established the plasma parameters required for a magnetic confinement fusion reactor [8], although not all parameters have been achieved simultaneously in a single plasma discharge.

For this reason, several countries are increasing their efforts to achieve commercial fusion capable of producing electrical energy as soon as possible. For example, the European consortium for fusion, EUROfusion, with its program [9] aims to reach this goal by 2050 through its flagship reactors ITER (tokamak type) [10] and Wendelstein 7-X (stellarator type) [11]. Both are experimental reactors, whose purpose is to generate knowledge and scientific evidence to be extrapolated and evolved for application in commercial DEMO (tokamak) [12] and HELIAS (stellarator) [13] reactors. The National Institute for Fusion Science in Japan has built a research reactor called the Large Helical Device (LHD, stellarator type) [14]. Across the ocean, the Plasma Science and Fusion Center at MIT is working on the ARC reactor (tokamak type) with high-temperature superconducting magnets [15].

Different paths are represented by different designs and choices of materials, but they all share the use of superconductivity to achieve magnetic confinement. Copper coils used so far in experiments can generate stationary magnetic fields as strong as two Tesla in very large volumes [16]. This comes at the cost of enormous amounts of energy since normal conductors dissipate current due to the Joule effect, which would have a huge impact on the energy balance of a commercial nuclear fusion reactor.

The need to develop large, reliable, high-field superconducting magnets has been recognized since the beginning, leading to the initiation of projects as early as the 1970s when superconducting wires became available on an industrial scale. For instance, superconductivity has proven to be an essential technology to improve and/or realize several high-energy particle projects. In the case of magnetic confinement fusion, superconducting magnets are the only viable solution for confining and shaping the plasma for prolonged burn periods.

Superconductivity is a physical phenomenon that occurs in certain materials under specific conditions. In the superconducting state, a material expels all magnetic fields from its interior, known as the Meissner effect [17], which has significant implications for creating stable and strong magnetic fields. Additionally, because of the superconducting state, a material offers zero resistance to the flow of electric current. This means that an electric current can circulate in a superconducting loop without energy dissipation and thus without electrical losses.

The superconducting state of a material depends, as seen in Figure 1.1 - 3, on the temperature, on the magnetic field in which the material is placed and the current density passing through it.
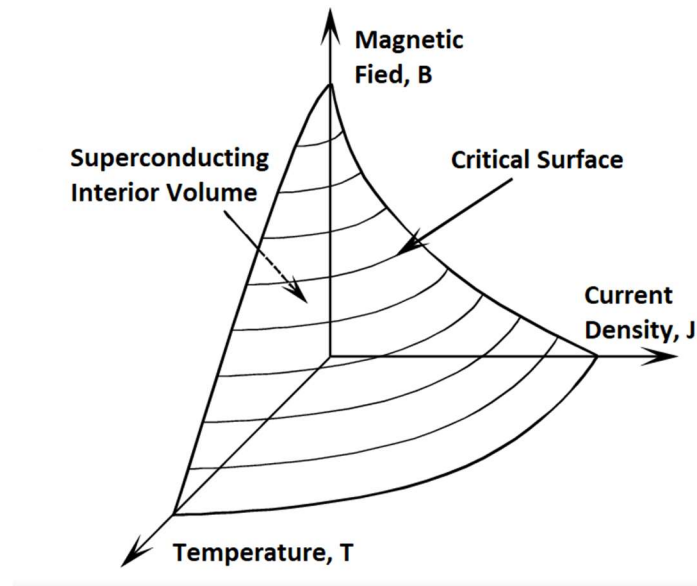
Figure 1.1 - 3: Schematic illustration of the critical surface that delimits the superconducting state of a material bounded by the critical temperature, critical current and critical magnetic field. Image adapted from [18].

Superconductors have a current density limit (critical current density), a temperature limit (critical temperature), and a magnetic field limit (critical field) beyond which they lose their superconducting properties. These parameters depend on the type of superconducting material chosen, and various designs have been proposed over the years, especially in the field of fusion. Section 1.2 aims to provide an overview of these designs.

1.2 Different cables and design

There are several distinctions that can be made between superconducting cables, one of which concerns the type of superconducting material they are made of. In this regard, there are two main families: Low-Critical Temperature Superconductors (LTS) and High-Critical Temperature Superconductors (HTS).

1.2.1 LTS cables

LTS cables were the first to be discovered and are primarily composed of metal alloys. The materials commonly used for these cables include NbTi (Niobium-Titanium) and Nb_3Sn (Niobium-Tin). Their name is due to the critical temperature that characterizes them, ranging from 10 K for NbTi to 23 K

for Nb$_3$Sn. For this reason, cables are designed to operate at around 4 K (-269°C), and the chosen coolant is supercritical helium (SHe).

They are structured with numerous very thin superconducting filaments, typically with diameters on the order of a few micrometers. The filaments are embedded in a matrix of copper or a copper alloy, which provides a path for the electric current in case the superconducting cable becomes resistive, also helping to dissipate the generated heat [19]. The superconducting filaments are often twisted to reduce the AC losses in case of pulse coils [20].

This design makes them relatively easy and inexpensive to construct [21], but costly to operate due to the need to cool them with supercritical helium. Their application is not limited to magnets for fusion reactors but also extends to particle accelerators [18] and medical devices such as MRIs [22].

An example of a Nb$_3$Sn ITER-like cable can be seen in Fig 1.2 – 1 that show how the filaments are wound into sub-cables, which are then twisted around an open central channel. Here, the coolant will be free to flow from the central channel to the peripheral channels by the winding of the filaments according to the hydraulic impedance of the paths:

Figure 1.2 – 1: Exposed view of a Nb$_3$Sn ITER-like cable for toroidal field coils. Images by Charlie Sanabria. SULTAN-tested cable was provided by courtesy of Pierluigi Bruzzone (Plasma Physics Research Center) with agreement from Fusion for Energy.

1.2.2 HTS cables

HTS cables are known for their superconducting properties at temperatures above 77 K (-196°C). They are primarily composed of ceramic materials known as high temperature cuprates. High temperature cuprates are complex oxides containing copper and other elements such as barium, thallium, mercury, or strontium. Compared to LTS, HTS exhibit higher values of critical temperature, critical magnetic field, and critical current density.

One of the primary challenges with these materials, is that they are ceramics, that makes them fragile and severely limits their flexibility. To overcome this issue, the filaments are encased in highly flexible silver metal. The resulting assembly is then flattened into a thick "tape" format, which is wound into the final cable configuration. In their shape, tapes are very different from the filaments used for LTS.

Among the most studied and used are REBCO conductors (for example, $YBa_2Cu_3O_7$), which consist of a layer of ceramic material about 1.0 μm thick deposited on a Hastelloy C-276 substrate 50 μm thick through metal-organic chemical-vapor deposition. A buffer of MgO is then inserted with ion-beam-assisted deposition. Another layer of silver 2-3 μm thick is deposited over the REBCO for thermal and electrical stability, and finally, the whole is surrounded by two layers of copper each 20 μm thick again for electrical and thermal stability [23].

The production of HTS cables requires advanced and complex techniques, which can lead to higher production costs and longer manufacturing times, affecting their large-scale adoption. Additionally, these tapes are made of ceramic material, so in any application, it is necessary to evaluate whether the strain values are acceptable [24].

On the other hand, their operation at a higher temperature and the ability to carry higher current densities, thereby increasing the magnetic field, is a very attractive prospect for many applications, including nuclear fusion [25].

For this reason, various configurations are being studied to maximize the advantages of these materials and the critical current density they can carry. To achieve this, multiple tapes of superconducting material are grouped together. Figure 1.2 – 2 lists a series of possible configurations, like the twisted stack tapes cables, Conductor on Round Core (CORC), and Roebel cables. The twisted stack tapes cable [26] is a cabling method suitable for developing a high-current cabled conductor for high-field magnet applications, such as fusion and accelerator machines. The CORC

cable [27] has great advantages on the easy fabrication, good mechanical stability, proper isotropic field characteristics, and the potential for the long-distance cabling. The Roebel cables [28] thanks to their structure can reduce the AC losses and for this reason they can be used in particular for AC current and ramped field.
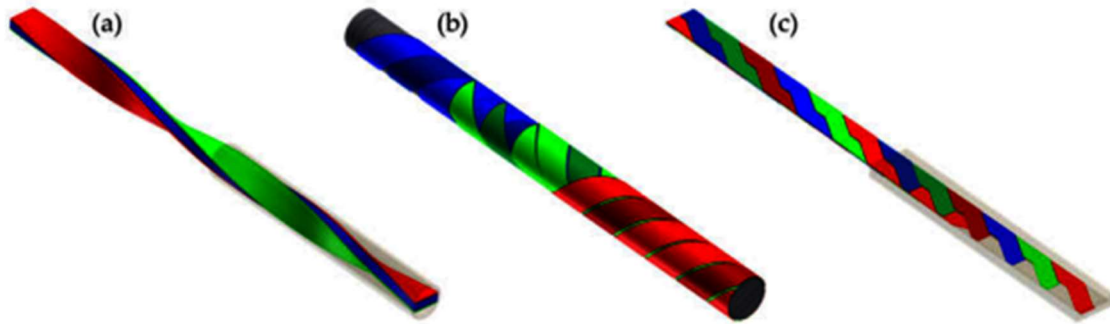

Figure 1.2 – 2: Various configurations of REBCO cables: a) Represents a Twisted Stacked Tape Cable (TSTC), b) Represents a Conductor on Round Core (CORC), and c) Represents a Roebel Cable. Image adapted from [29]*.*

Besides the arrangement of tapes, there are various designs of cooling channels, cable geometries, and materials used alongside the tapes. Figure 1.2 - 3 illustrates cross-sections of three different TSTCs and describes their characteristics. For example, the ENEA cable utilizes a central coolant channel with each tape stack surrounded by two smaller lateral channels. There's also the design from the Karlsruhe Institute of Technology [30], featuring a stabilizing sheath around each tape stack with a central stabilizing copper cable and coolant surrounding it. Another design by North China Electric Power University [31] attempts to achieve an isotropic tape stack model by positioning tapes both vertically and horizontally.
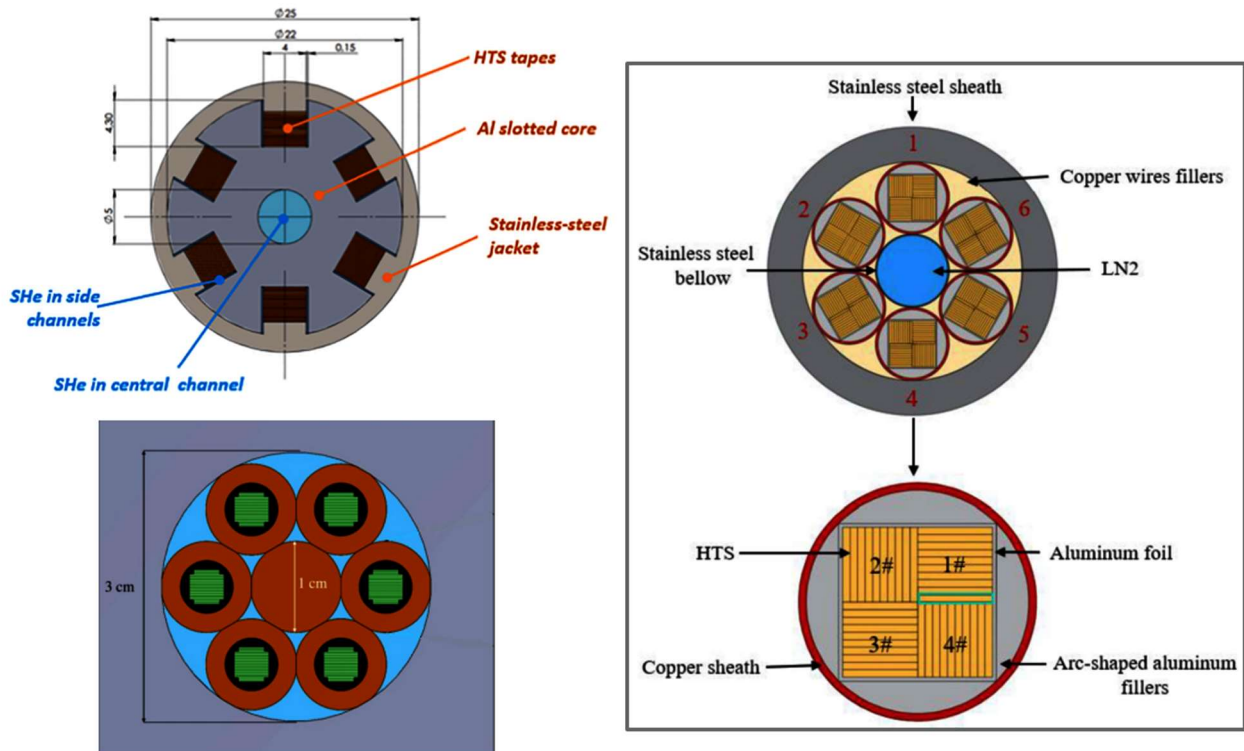
Figure 1.2 – 3: Cross sections of different TSTCs. In the top right, we see an ENEA cable. In the bottom right, a cable by the Karlsruhe Institute of Technology. Image adapted from [30]. *On the left, the cable proposed by North China Electric Power University. Image adapted from* [31].

1.3 Modeling SC cables

As seen in section 1.2, cable designs can vary significantly, and in studying their behavior, it is essential to consider the coupled mechanical, electrical, thermal, hydraulic and even nuclear physics. In other words, the modeling of SC cable is a multi-physic problem.

In the event of a quench, for example, the superconductor will redistribute the current into the stabilizing materials of the cable. These materials, being normal conductors, will dissipate current through the Joule effect, becoming sources of heat. This heat must be removed by the fluid part of the system, which will experience changes in its fluid dynamic conditions.

These interactions between different phenomena, although extremely important to understand and control, are very difficult to interpret without the appropriate simulation tools [32]. For this reason, many software programs have been developed over the years, particularly for forced-flow applications, which are well-established especially for LTS cable analysis.

8

The remainder of this section is an introductory, not exhaustive, overview of the most established software for the thermal-hydraulic and electrical modeling of superconducting cables for forced flow applications, the 4C code, the THEA code and the VINCENTA/VENECIA code.

The 4C code (Cryogenic Circuit Conductor and Coil) is a proprietary software [33], developed since 2008 by the Energy Department of the Politecnico di Torino. In recent years, it has achieved excellent results both in terms of validation (comparison with experimental data) and benchmarking (comparison with data from other software). It can perform steady state and transient simulations for thermal, hydraulic, and electrical analyses of SC cables and magnets. It has a modular structure, and each module is then coupled with the others. In this module This module employs first-order Finite Element Method (FEM) for spatial discretization using an adaptive grid. It utilizes either an implicit scheme (such as Backward Euler, BE) or a semi-implicit scheme (like Crank-Nicholson, CN) for time integration, offering up to second-order accuracy. The time stepping can be adapted to accurately capture abrupt changes in cable transients.

One module is dedicated to the 1D thermal-hydraulic model for the winding pack and channels that cool any enclosures. In this "multi-conductor" model, each conductor is simulated using Multi-conductor Mithrandir code (M&M) [34], which uses FORTRAN as the programming language.

The second module contains a 2.5D heat conduction model for structural solid components, such as radial plates (those that form the "skeleton" of a superconducting magnet). This module is implemented using a programming language like FreeFem++.

The third module contains the 0D circuit model of the hydraulic circuit, implemented using object-oriented a-causal model in Modelica [35].

Recently, the 4C codes have also been expanded with a model for HTS cables (H4C [30]), which includes a distributed parameter model for the electrical model, but it is not suitable for modeling LTS because it has a simplified treatment of the coupling between the channels.

The THEA/SUPERMAGNET code [36] couples a thermal-hydraulic model with an electrical model, both with distributed parameters. The electrical equations of the model are derived from the magneto-quasi-static formulation of Maxwell's equations. The thermal-hydraulic model solves the 1D conservation equations of mass, momentum, and energy for the coolant (supercritical He) in the non-conservative variables of velocity, pressure, and temperature, and the conservation of energy for the solid elements.

THEA code can model an arbitrary number of solid and fluid components. There is also a 0D model for the hydraulic circuit. It uses finite elements with adaptive mesh and a multi-step adaptive method for time advancement.

VICENTA/VENECIA is another commercial code for [37] conducting thermal-hydraulic studies. Its range of applications is vast, including many devices such as those for nuclear fusion but also Magnetic Resonance Imaging (MRI) magnet systems, superconducting motors and generators, among others. It offers great flexibility in the choice of coolant, allowing for circuits with helium (superfluid, supercritical, or a two-phase mixture), nitrogen, hydrogen, oxygen, neon, or water. The code's architecture includes various modules, each described by its own mathematical set of equations (algebraic or differential), representing the components of the system to be simulated (SC cables, pumps, valves, etc.). Also in this case, the conservation laws for fluids are discretized in 1D and solved using the finite difference method with accuracy up to the 5th order. A semi-implicit method is used for time integration. This code was also used for time-dependent thermal-hydraulic analyses of the ITER toroidal field [38].

In this context, another code was developed, called OpenSC^2, which from the beginning has been designed to simply discretize both LTS and HTS cables, regardless of their use, whether in nuclear facilities or power transmission. It is an open-source code developed in Python [39] following object-oriented programming principles. Being OpenSC^2 the tool used in this thesis work, Chapter 2 will extensively discuss its features.

1.4 Objectives and structure of the thesis

The main aim of the thesis is to verify the correct implementation and behavior of the lumped electric model recently implemented in OpenSC^2 [40] and coupled with the thermal hydraulic model. Being a first step in the verification of the electric model and of its coupling with the thermal hydraulic one, a benchmark against the results obtained with the 4C code is carried out. The goal is twofold: on the one hand to compare and assess the difference between the results obtained with OpenSC^2 against the outcomes of the 4C code; on the other hand, to ensure that the redistribution of the current satisfies the physics of the system. Specifically, it is essential to verify that the superconducting cable redistributes the current within it at the onset of quenching as predicted by the electrical model.

With this in mind, the electric model is tested against a transient characterized by a significant current redistribution: the current, that in nominal operating conditions is carried by superconducting components, is then shared with other current carriers that composed the cable but made with normal

conductors like copper or aluminum. In these conditions, the flow of current through materials with a non-zero electric resistance triggers the heat deposition by Joule effects in those components. This inner heat generation influences the thermal-hydraulic behavior of the heat sink (the coolant) as well as the thermal response of all the solid materials. This transient is therefore a perfect candidate for verification as it intrinsically requires the modeling of both the physics involved.

The remainder of the thesis is structured as follows.

In Chapter 2 the thesis will present a brief explanation of how to model a cable using the OpenSC^2 software, describing both the thermal-hydraulic and the electric models, with more emphasis on the latter, together with their coupling strategy.

Chapter 3, on the other hand, will present the actual case study, the reasoning that went into fitting the input data of the problem into the new software, the changes that had to be made to the code to better model the case study, the verification of the solution, and the results obtained from the benchmark. Subsequently, there is an analysis of the results obtained and a comparison of the differences between the calculations obtained with the 4C model and those obtained with OpenSC^2. Finally, Chapter 4 summarizes the conclusions of the work done and outlines some future prospects for achieving even better results from the use of OpenSC^2.

2 Modeling SC Cables with OpenSC^2

Chapter 1 introduced some useful codes to evaluate different transients for superconducting cables. The focus of this chapter is to describe the OpenSC^2 code, and in particular to highlight:

- What it can do;
- How the cable is discretized;
- How the electrical model works;
- The thermal-hydraulic model;
- The coupling between the electrical model and the thermohydraulic model.

OpenSC^2 is a software for the multi-physical analysis of thermal-hydraulic and electro-dynamic transients in Superconducting Cable-in-Conduit Conductors (CICC) for fusion magnets and power transmission. It adopts an open-source approach, promoting widespread use and enabling the testing of various configurations. This broad usage helps to highlight both the strengths and the unresolved or unidentified issues.

2.1 Introduction

According to [39] the software is designed for both steady-state and transient analyses of CICC (Cable-in-Conduit Conductors) under operating conditions. It can handle cables composed of Low Temperature Superconductors (LTS), such as Nb$_3$Sn and NbTi strands, as well as High Temperature Superconductors (HTS) tapes made from various materials. Users can select different coolants and cooling configurations to suit their specific needs. The software is particularly valuable for studying steady-state operating conditions under environmental parasitic loads, as well as transient operations including current variation over time, coolant flow variation, AC losses, quench events, fast discharges, and fault currents. It also aids in the research for optimal configurations within a set of constraints, allowing users to evaluate the temperature margin to current sharing along cables in predefined operating scenarios.

OpenSC^2 is entirely written in Python, and before starting the simulation, the user must provide input data to configure the simulation features. This includes building the conductor and its fundamental components, constructing the grid, setting the drivers, defining the cable topology and interfaces, and, lastly, compiling the diagnostics to save the output. This process is facilitated by appropriate input

files in the form of Excel spreadsheets (.xlsx), which must be completed before each run. An overview of the input files and instructions on how to complete them will be presented in Appendix A.

2.2 OpenSC² architecture

The software is designed according to the principles of Object-Oriented Programming (OOP) [41]. To evaluate the behavior of a superconducting cable and its evolution over time, it is therefore evaluated as composed of individual objects. The superconducting cable is referred to as a "conductor" in the code and will be referred to as such in this text.

Each of these objects can be characterized by properties, i.e., the data associated with it, and behaviors, i.e., the operations it can perform. This approach is particularly useful for representing complex concepts and for facilitating software management and maintenance. Objects in code are constructed using classes, which are models that define the properties and behaviors common to a group of objects. A class describes a type of object by specifying the attributes (variables) and methods (functions) that each object of that class will have. Inheritance, supported by Python, allows one class to inherit attributes and methods from another class. This encourages code reuse and the creation of class hierarchies.

Within the code, the cable is thus organized as follows: there is a Simulation class that encapsulates all the properties and behaviors of the transient to be studied. Instead, another class, Conductor, called from within Simulation, is responsible for using the classes within the code to generate the instances, the objects that make up the SC cable. It evaluates the topology, evaluates the interfaces between components, builds the incidence matrix of the various current-carrying components, builds the electrical resistance matrix, and generally builds the stiffness matrix of the electrical model.

Within Conductor, two other classes are invoked: Fluid Component and Solid Component. The mathematical model that describes their behavior will be explained in section 2.4, but for now we can generally say that these two classes create the fluid objects and the solid objects. Through the principle of inheritance that characterizes the Python language, the Solid Component class is again extended into two classes, Strands and Jacket, the latter modeling solid components that are not involved in current transport. The Strands class is further extended into Stabilizer to model the non-superconducting conductor components, Strand Mixed to model filiform components such as LTS cables for fusion magnets (but also MgB2 cables for power transport), and Stack to model components made from a set of SC tapes, such as those made from HTS material (but MgB2 can also be used to make tapes).

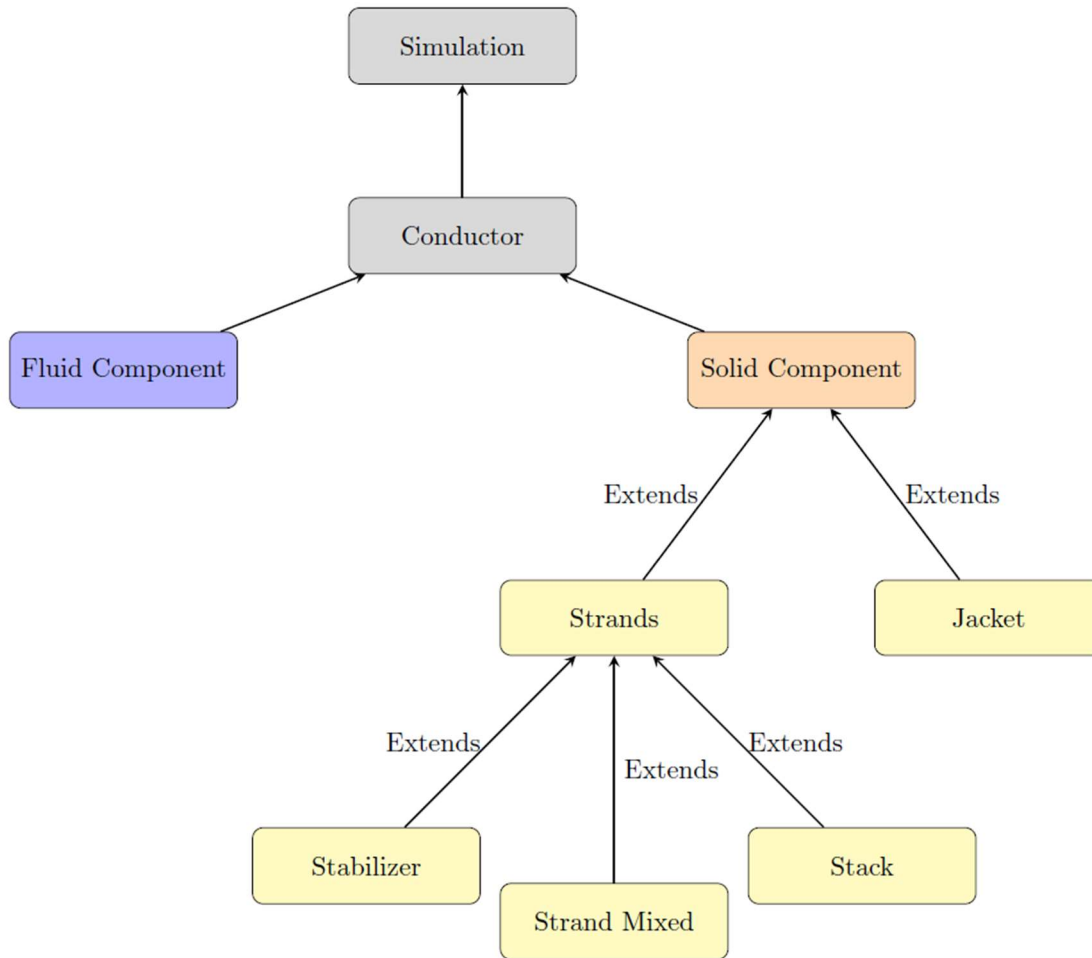The Figure 2.2 - 1 shows the hierarchy of the classes used in OpenSC^2.

Figure 2.2 – 1: Diagram of the relationship between classes. It also shows the inheritance concept that allows the extension of the Solid Component class into different classes that generate the instances that make up the cable. Strands class is for current carriers, while Jacket class is for material not involved in current transport. Strand Mixed and Stack classes model the SC current carriers.

The user of the software will then have to discretize, through the input files, the objects that will finally compose the cable.

Through the classes presented in Figures 2.2 – 1, it is possible to represent 3 main different types of objects, as also described in [42] and visible in Table 2.2 – 1:

Table 2.2 – 1: Schematic view of the object in which the conductor can be discretized. The symbols of the objects are adapted from [42].

Symbol	Object
	Strands Object SO
	Jacket Object JO
	Fluid Object FO

Each object has its own constitutive relationships (e.g., friction factors for FO) and connections to other objects (e.g., heat transfer coefficients).

The fluid components are associated with the Euler equations associated with the thermos-fluid dynamic model described in Section 2.4.1; the solid components (strand and sheath) are associated with the heat equation associated with the thermos-fluid dynamic model (Section 2.4.2). Also associated with the strand components are the electrical model equations discussed in section 2.3.

2.3 Electrical Model

The mathematical model [43] is based on a lumped element equivalent circuit, which accounts for the interactions between current-carrying elements through longitudinal electrical resistances, self and mutual inductances, and transverse conductances between the different strands or tapes, depending on the cable layout. One-dimensional elements with arbitrary orientation in 3D space are employed to represent the cable geometry. These elements can include both active components, which have a transport current applied by external sources, and passive components, where only eddy currents are present.

2.3.1 How the model is built

Each SOs object is discretized in its length into a series of nodes, and between two consecutive nodes of each object there will be a side characterized by a certain resistance R and inductance L.

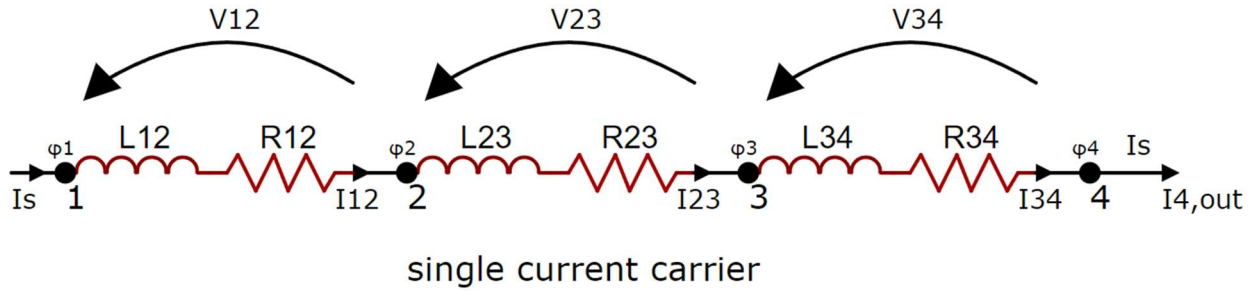An example of a cable divided into 4 nodes is described in Figure 2.3 - 1:

Figure 2.3 – 1: Example of cable discretization for the electrical model for a single current carrier

In the example problem, I_s is known and represents the source current flowing along the current carrier. The unknowns are 8 and are represented by the 4 electric potentials, one at each node, and the 4 outgoing currents from each node.

When Kirchhoff's laws are applied to a scheme such as that in Figure 2.3 - 1, 7 equations can be written, so that in addition to the external current applied to the circuit, the electrical potential value for an equipotential surface of the cable, one of the nodes, must also be imposed. The potential is defined by an arbitrary constant, and by setting this value you are actually defining the value of that constant.

In this way, the unknowns become 7, for the 7 Kirchhoff equations. 3 of these equations concern the voltage on the edges (Kirchhoff's second law):

$$V_{12} = R_{12}I_{12} = \varphi_2 - \varphi_1$$

$$V_{23} = R_{23}I_{23} = \varphi_3 - \varphi_2 \qquad\qquad (2.3 \text{ - } 1)$$

$$V_{34} = R_{34}I_{34} = \varphi_4 - \varphi_3$$

Three of these equations concern the voltage difference on the sides. To write equations (2.3 - 1) in compact form, it may be useful to introduce the incidence matrix $[A_e]$, which has the dimension m x n, where m is the number of sides and n is the number of nodes in the problem. The possible values for the generic elements $A_{e,ij}$ of the incident matrix are:

$$A_{e,ij} = \begin{cases} +1 & if\ edge\ e_j\ enters\ node\ n_i \\ -1 & if\ edge\ e_j\ leaves\ node\ n_i \\ 0 & otherwise \end{cases} \qquad (2.3\text{ - }2)$$

In this case, considering just one current carrier we can write the matrix as Table 2.3 – 1:

Table 2.3 – 1: Matrix A_e, the incidence matrix edge-to-node

	Node 1	Node 2	Node 3	Node 4
Edge 1	-1	+1		
Edge 2		-1	+1	
Edge 3			-1	+1

It is therefore possible to write the matrix system:

$$[R]\{I\} = [A_e]\{\varphi\} \qquad (2.3\text{ - }3)$$

With $[R]$ diagonal matrix.

The other 4 equations will be for currents passing through nodes (Kirchhoff's first Law):

$$I_s - I_{12} = 0$$

$$I_{12} - I_{23} = 0$$

$$I_{23} - I_{34} = 0 \qquad \text{(2.3 - 4)}$$

$$I_{34} - I_{4.out} = 0$$

Which can be written as:

$$-[A_e]^T\{I\} = 0 \qquad \text{(2.3 - 5)}$$

In the case where the cable has current flowing through it, the result will be the source current vector $\{I_S\}$.

Writing everything together in a single matrix system, and imposing the potential at 0, there will be:

$$\begin{bmatrix} R & A_e \\ -A_e{}^T & 0 \end{bmatrix}\begin{Bmatrix} I \\ \varphi \end{Bmatrix} = \begin{Bmatrix} 0 \\ I_S \end{Bmatrix} \qquad \text{(2.3 - 6)}$$

To make the model more realistic, inductances (already introduced in Figure 2.3 - 1) should be added to the resistors in the calculation.

In this case writing the equation of the voltage difference along edge V_{12} becomes:

$$V_{12} = \varphi_1 - \varphi_2 = R_{12}I_{12} + L_{12}\frac{\partial I_{12}}{\partial t} + L_{12,23}\frac{\partial I_{23}}{\partial t} + L_{12,34}\frac{\partial I_{34}}{\partial t} \qquad \text{(2.3 - 7)}$$

The complete system, also including contributions from the variable current will become:

$$\begin{bmatrix} L & 0 \\ 0 & 0 \end{bmatrix}\frac{\partial}{\partial t}\begin{Bmatrix} I \\ \varphi \end{Bmatrix} + \begin{bmatrix} R & A_e \\ -A_e{}^T & 0 \end{bmatrix}\begin{Bmatrix} I \\ \varphi \end{Bmatrix} = \begin{Bmatrix} 0 \\ I_S \end{Bmatrix} \qquad \text{(2.3 - 8)}$$

With [**L**] full matrix, because it contains the self-inductances on the main diagonal but also the mutual inductances.

For complex cable designs, a more sophisticated approach is required to accurately model their behavior (as discussed in detail in section 1.2). In general, a simple model based on a single set of inductances and resistances is insufficient to capture the full physics of the problem. The real physics of the problem becomes even more complicated when there are multiple current-carrying elements. In such cases, the current may be transferred from one conductor to another, or it may be distributed among several conductors. Therefore, it is essential to introduce multiple sets of inductances and resistances that are interconnected by conductances. This allows a more accurate representation of the current flow between different branches of the network, taking into account the complex interactions and current distributions within the cable.

If, for example, we consider two current carriers instead of just one, we can discretize the cable as in the Figure 2.3 - 2:
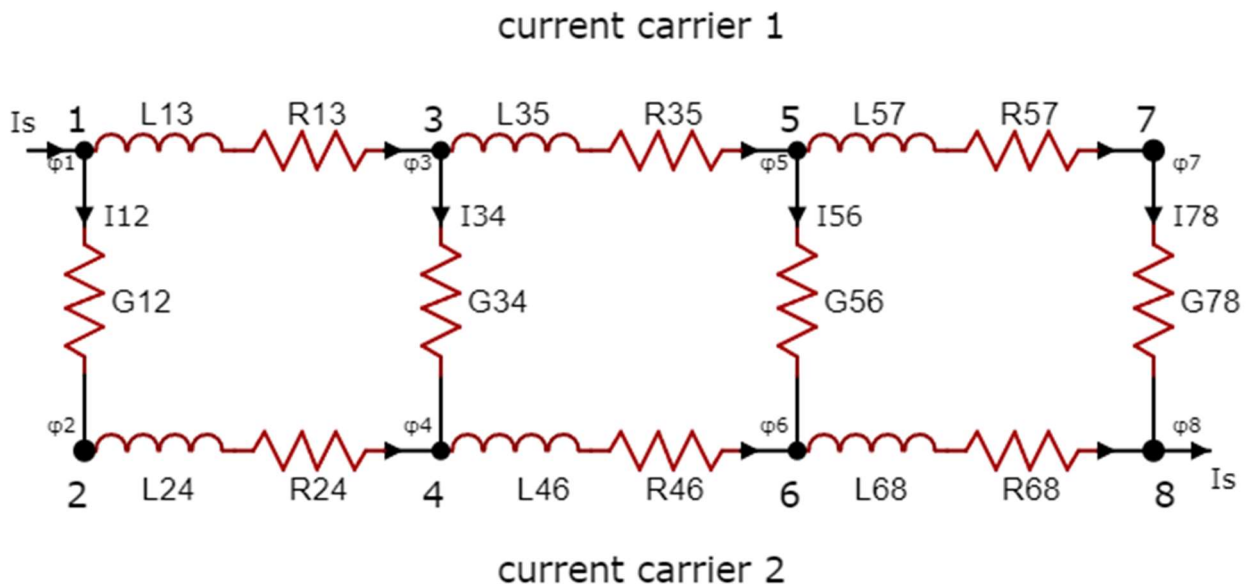

Figure 2.3 - 2: Example of a network of two longitudinally discretized current carriers with series of resistors and inductances and connected to each other (because they are in electrical contact) by conductances.

The edges of the same current carrier have not changed, while new equations on the nodes are added. We can write the new equations as:

$$I_{12} = \frac{V_{12}}{R_{12}} = G_{12}(\varphi_2 - \varphi_1)$$

$$I_{34} = \frac{V_{34}}{R_{34}} = G_{34}(\varphi_4 - \varphi_3)$$

(2.3 - 9)

$$I_{56} = \frac{V_{56}}{R_{56}} = G_{56}(\varphi_6 - \varphi_5)$$

$$I_{78} = \frac{V_{78}}{R_{78}} = G_{78}(\varphi_8 - \varphi_7)$$

Equations 2.3 – 9 model the sharing of the current between the current carriers, that causes a voltage difference between nodes on the same coordinate.

Writing everything together, including the previous information regarding the current entering or exiting in each node there will be:

$$-[A_e]^T\{I\} + [G]\{\varphi\} = \{I_S\}$$

(2.3 - 10)

We can call $[G]$ the sparse conductance matrix, which contains the contact conductance. This matrix is fundamental to the electrical model because it describes the electrical connections between nodes of the current carriers on the same cross section. Thus, the final system that solves the circuit can be rewritten as:

$$\begin{bmatrix} L & 0 \\ 0 & 0 \end{bmatrix} \frac{\partial}{\partial t} \begin{Bmatrix} I \\ \varphi \end{Bmatrix} + \begin{bmatrix} R & A_e \\ -A_e^T & G \end{bmatrix} \begin{Bmatrix} I \\ \varphi \end{Bmatrix} = \begin{Bmatrix} 0 \\ I_S \end{Bmatrix}$$

(2.3 - 11)

This system is solved by writing the global stiffness matrix of the problem and entering the initial conditions, which are as mentioned in the course of the discussion the vector of source currents $\{I_S\}$ and the value of an equipotential surface of the cable.

In the general case of multi-current carriers there is the need to define the equipotential surfaces. Let focus on the simplest case of two current carriers and consider the first slice of the discretization where the current is entering the conductor. A possible way to model this specific situation is shown in Figure 2.3 – 3 a, where the current enters in the conductor through the artificial node 0 and then it redistributes through connections 01 and 02. It should be noted that those connections are shortcuts, i.e. no resistivity nor inductances are associated with them, meaning that the surface where those nodes are placed is characterized by no voltage difference, i.e. it is equipotential. Therefore, the scheme of Figure 2.3 - 3 a is equivalent to the scheme shown in Figure 2.3 – 3 b where the artificial node 0 is removed and the current enters directly into one of the nodes 1 and 2 (by convention node 1). The same rationale applies to the last cross section of the conductor, where the current flows out of the conductor. The model treats this surface as equipotential.

As a final remark, it should be discussed the definition of the reference value for the voltage, that allows to reduce the number of unknowns by m (if m is the number of current carriers). It will be assigned to one of the two equipotential surfaces and conventionally the reference value is set to 0; Figure 2.3 – 3 show this for the equipotential surfaces at the beginning of the conductor.

Equation 2.3 – 11 is a set Algebraic Differential Equations that is solved converting the ODE in an algebraic equation applying an implicit method (Backward Euler of Crank Nicolson) and then solving the resulting algebraic set of equation with a direct solver.
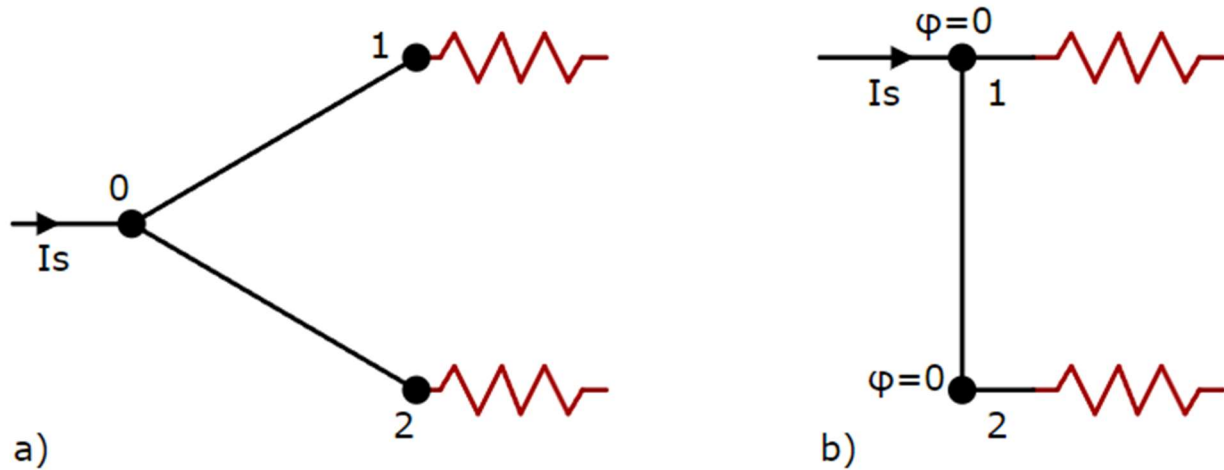
Figure 2.3 – 3: Diagram illustrating why the first surface of the conductor can be considered equipotential; a similar representation can be made for the last surface of the conductor. In (a) a formal schematic is shown, in (b) a compact and equivalent representation is shown by eliminating the shorts 01 and 02 found in (a). Also shown in b) is the reference value assigned to the potential, which by convention is set equal to 0.

Once currents and potentials at each node have been evaluated, one has all the tools to be able to calculate the power by Joule effect generated within the conductor, evaluated as the integral over time of the potential difference multiplied by the current:

$$Q_{Joule} = |\Delta\varphi| * I * \Delta t \qquad\qquad (2.3\text{-}12)$$

Equation 2.3 - 12 is general and can be applied to evaluate both the contribution to the Joule power due to the voltage difference and current in each edge and the contribution to the Joule power due to the voltage difference and current across current carriers. The Q_{Joule} parameter will represent, as described in the Section 2.4.2, a source term in the temperature equation for solids.

2.3.2 Focus on the R matrix

This section purpose is to clarify the construction of the electric resistance matrix in OpenSC², one of the key points of the electric model.

Generally speaking, the electric resistance of a material is expressed by:

$$R = \rho_{el} \frac{l}{A_{Str}} \tag{2.3 - 13}$$

where the subscript Str stands for Strand Object and ρ_{el} is the specific electrical resistivity of various materials as a function of temperature. Equation 2.3 - 13 is used directly to evaluate the electric resistance of Stabilizer object in OpenSC^2 which is provided by a library of properties for the most commonly used materials, including their electric resistances.

Things get more involved when considering object used to model SC materials. Indeed, in OpenSC^2, both classes that handle superconducting materials (Strand Mixed and Stack classes, as seen in Figure 2.2 - 1) assume that these are thermally and electrically coupled with other non-superconducting materials. Because the material properties are homogenized, the electrical properties must also be managed accordingly.

In this context, it is essential to consider the current divider effect between the electrical resistance of the SC material and that of the non-SC material. The homogenization process ensures that the combined properties reflect the contributions of both types of materials. This means that the overall electrical behavior of the system is influenced by the interplay between the low resistance of the SC components and the higher resistance of the non-SC components that is modelled by the equivalent resistance of the electric parallel between these materials.

The current divider concept is crucial here: when current flows through a Strand Mixed or a Stack object, it splits between the SC paths and the non-SC paths based on their respective resistances. In nominal operating conditions, the SC material, with its minimal resistance, will carry a significant portion of the current, while the non-SC material, with its higher resistance, will carry less. Under off-normal conditions (such as quenching) the electrical resistivity of the SC materials becomes orders of magnitude greater than that of the non-SC materials, so the current will flow through these materials generating Joule power. This division of current is essential for accurately modeling the electrical performance of the material under various operating conditions.

Understanding and correctly implementing this current partitioning is vital for predicting the behavior of the cable in real-world applications, where both superconducting and non-superconducting elements interact to affect the overall performance.

The electrical resistivity for SC materials usually is evaluated using the power law:

$$\rho_{el,sc} = \frac{E_0}{J_c}\left(\frac{J_{sc}}{J_c}\right)^{n-1} \tag{2.3 - 14}$$

As can be seen within the formula appears J_{sc}, which is the current density flowing directly into the superconducting part of the object which is obtained from the solution of the current divider. Thus, the problem is implicit and strongly not linear due to the large value of the exponent n (tipycally $>$ 10).

Therefore, to obtain the electrical resistivity of the superconducting object, a nonlinear set of equations must be solved must be solved:

$$\begin{cases} \Delta\varphi_{sc} = R_{sc}\,I_{sc} = \rho_{el,sc}\dfrac{l}{A_{sc}}I_{sc} = E_0\dfrac{l}{A_{sc}}\left(\dfrac{J_{sc}}{J_c}\right)^{n-1}\dfrac{A_{sc}}{I_c}I_{sc} = E_0l\left(\dfrac{J_{sc}}{J_c}\right)^{n} \\ I_{Str} = I_{notSC} + I_{sc} \rightarrow I_{notSC} = I_{Str} - I_{sc} \end{cases} \tag{2.3 - 15}$$

Now we can equalize the potential difference between the two nodes by obtaining:

$$(I_{Str} - I_{sc})\frac{\rho_{el,notSC}}{A_{notSC}}l = E_0l\left(\frac{J_{sc}}{J_c}\right)^{n} \tag{2.3 - 16}$$

Hence normalizing the current density over the total area of the superconducting object will give:

$$I_{sc}{}^{n} + (I_{sc} - I_{Str})\frac{\rho_{el,notSC}}{A_{notSC}E_0}I_c{}^{n} = 0 \tag{2.3 - 17}$$

At this point OpenSC^2 calculates the current I_{sc} by the Newton-Halley method and uses the current so calculated to calculate the electrical resistivity of the superconducting material.

$$\rho_{el,sc} = \frac{E_0}{J_c}\left(\frac{I_{sc}}{I_c}\right)^{n-1} \tag{2.3 - 18}$$

24

Known the electrical resistivity of the SC, applying equation 2.3 – 13 the code computes the electric resistance of the SC; finally, the equivalent resistance of the parallel between the R_{SC} and R_{non_SC} is computed and this value is inserted into the $[\boldsymbol{R}]$ matrix to build the global stiffness matrix and solve the current model.

2.4 Thermohydraulic model

In this section, the thermohydraulic model of OpenSC^2 will be represented, and in particular we will look at:

- the equations governing the behaviour of Fluid Objects FOs;
- the equations governing the behaviour of Solid Objects SOs and JOs;
- the connections provided by the software between the objects;
- the coupling of the equations.

2.4.1 Mathematical model for Fluid Component

Within the Fluid Component class, the code solves the conservation equations of mass, momentum and energy in 1D. Expressed in their conservative form they led to the following system:

$$
\begin{cases}
\dfrac{\partial \rho}{\partial t} + \dfrac{\partial \rho v}{\partial x} = \Lambda_\rho \\[2mm]
\dfrac{\partial \rho v}{\partial t} + \dfrac{\partial \rho v^2}{\partial x} + \dfrac{\partial p}{\partial x} = \Lambda_v \\[2mm]
\dfrac{\partial \rho e}{\partial t} + \dfrac{\partial \rho e v}{\partial x} + \dfrac{\partial p v}{\partial x} = \Lambda_e
\end{cases}
\qquad (2.4\text{ - }1)
$$

This writing, however, as mentioned in [44], is not always preferable, however much it guarantees numerical conservation of all flows. The former form makes it possible to derive velocity, density, and specific energy of the fluid directly, but at each instant of time temperature and pressure must also be derived explicitly, and this greatly burdens the computational cost. Therefore, the implicit form described in [34] was used:

Each channel is thus modeled through its set of Euler-like equations.

$$\begin{cases} \dfrac{\partial v}{\partial t} + v\dfrac{\partial v}{\partial x} + \dfrac{1}{\rho}\dfrac{\partial p}{\partial x} = \dfrac{1}{\rho}\left(\varLambda_v - v\varLambda_\rho\right) \\[2mm] \dfrac{\partial p}{\partial t} + \rho c^2\dfrac{\partial v}{\partial x} + v\dfrac{\partial p}{\partial x} = \varPhi\left[\varLambda_e - v\varLambda_v - \left(w - \dfrac{v^2}{2} - \dfrac{c^2}{\varPhi}\right)\varLambda_\rho\right] \\[2mm] \dfrac{\partial T}{\partial t} + \varPhi T\dfrac{\partial v}{\partial x} + v\dfrac{\partial T}{\partial x} = \dfrac{1}{\rho c_v}\left[\varLambda_e - v\varLambda_v - \left(w - \dfrac{v^2}{2} - \varPhi c_v T\right)\varLambda_\rho\right] \end{cases} \qquad (2.4\text{ - }2)$$

This is a set of partial differential equations (PDEs) in time and space, coupled by the fact that the velocity term appears in all three equations, while the pressure term appears in the first two. The set of equations is thus nonlinear, as can be seen, for example, from the term $v\dfrac{\partial}{\partial x}$ or the fluid properties (ρ, c, c_v or $\varPhi$), which being functions of both pressure and temperature will necessarily be nonlinear. The right-hand side of the equations encloses the source terms, constructed by combining the various $\varLambda$, which are: $\varLambda_\rho$ (mass source), $\varLambda_v$ (momentum source) and $\varLambda_e$ (energy source). For more information on these terms, refer to [45].

To solve the system of equations, initial conditions and a set of boundary conditions to be provided in the input file through a flag are obviously needed for each channel one wants to model. Three different sets of BCs are currently provided, which are:

1. User supplied input pressure, output pressure and input temperature;
2. User supplied input pressure, input temperature and output mass flow;
3. User-supplied inlet mass flow, inlet temperature, and outlet pressure.

Each fluid object is thus modeled through its set of Euler-like equations.

2.4.2 Mathematical model for Solid Component

The solid components are modeled with the Cartesian transient heat equation 1D.

The following equations are given for both the generic Strand Object (subscripted Str) and the generic Jacket Object (subscripted JO) since these have very similar equations if we look at the left side of the equation but differ slightly for the right side. In fact, for the jacket, there is a unique thermal interface with the external environment (env), the characteristics of which can be provided from input files. Additionally, jacket objects could also experience radiative heat transfer, which must be accounted for in the thermal modeling.

$$A_{Str}\rho_{Str}c_{p,Str} - A_{Str}\frac{\partial}{\partial x}\left(k_{Str}\frac{\partial T_{Str}}{\partial x}\right)$$

$$= \sum_{ch=1}^{N_{ch}} P_{Str,ch}h_{Str,ch}(T_{ch} - T_{Str}) + \sum_{st\neq fi}^{N_{st}} P_{Str,st}h_{Str,st}(T_{st} - T_{Str})$$

$$+ \sum_{jk=1}^{N_{jk}} P_{Str,jk}h_{Str,jk}(T_{jk} - T_{Str}) + Q_{Str,Joule} + Q_{Str,ext} \qquad (2.4\text{ - }3)$$

$$A_{JO}\rho_{JO}c_{p,JO} - A_{JO}\frac{\partial}{\partial x}\left(k_{JO}\frac{\partial T_{JO}}{\partial x}\right)$$

$$= \sum_{ch=1}^{N_{ch}} P_{JO,ch}h_{JO,ch}(T_{ch} - T_{JO}) + \sum_{st=1}^{N_{st}} P_{JO,st}h_{JO,st}(T_{st} - T_{JO})$$

$$+ \sum_{jk\neq i}^{N_{jk}} P_{JO,jk}h_{JO,jk}(T_{jk} - T_{JO}) + Q_{JO,ext} + P_{env,JO}h_{env,JO}(T_{env} - T_{JO}) \qquad (2.4\text{ - }4)$$

The cross-section, density, specific heat, and thermal conductivity are calculated considering that both strands and jackets are typically composed of multiple materials. For example, strands may consist of superconducting filaments embedded in a matrix of stabilizing material, usually copper, while jackets might be made of stainless steel and glass-epoxy insulation.

These equations are primarily characterized by their parabolic nature and the inherent non-linearity due to terms like $\rho c_p \frac{\partial T}{\partial t}$ and $k\frac{\partial T}{\partial x}$. These thermophysical properties are temperature-dependent and generally non-linear. Additionally, there are coupling terms with other solids and/or channels that contribute to the right-hand side of the equations, along with external drivers. To solve the equation for each solid component, initial conditions must be specified, and one inlet and one outlet boundary condition need to be applied. OpenSC^2 applies initial temperature of solid components and homogeneous Neumann (adiabatic) boundary conditions.

As illustrated by the equations, there are two types of heating sources: the power generated by the Joule effect (Q_{Joule}) and the external heating (Q_{ext}). Joule heating arises from the loss of superconductivity in the strands or because a portion of the current might be carried by non-superconducting solids under off-normal operating conditions, and it is calculated as described in
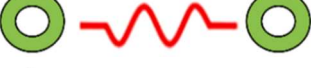
Section 2.3. In experimental settings, external heaters are typically used to induce the transients of interest in superconducting cables, such as simulating parasitic heating or quench phenomena. In OpenSC^2, the ability to assign an external power source as a driver allows for the replication of conditions recreated during experiments. This external heating acts as a linear power source introduced into the strands, serving as a crucial driver for studying superconducting cable transients. By applying external power, OpenSC^2 can accurately simulate the effects observed in laboratory experiments, thereby enhancing the reliability and relevance of the simulation results.

2.4.3 Connections between objects

So far, we have seen how the mathematical model of fluid objects and solid objects is constructed. Once the different instances have been created, and thus the different objects have been constructed, it is important to define how they are connected to each other in order to substantiate the source terms present in the Euler equations for fluids and in the conservation of energy for solids. In fact, depending on the type of connection, there will be, for example, a different heat transfer coefficient between one object and another (denoted by h in the equations 2.4 – 3 and 2.4 - 4), or sources of pressure, temperature or velocity if the conductor has a hydraulic parallel (see the chapter on LTS cables).

From [42] we can summarize the various types of connections with the Table 2.4 – 1:

Table 2.4 - 1: Type of connections that can be modelled with OpenSC². The symbols of the objects and of the type of connection are adapted from [42].

Type of connection	Description	Object Involved
	Thermal by conduction	SO and SO
	Thermal by conduction	SO and JO
	Thermal by conduction	JO and JO
	Thermal by radiation	JO and JO
	Thermal by convection	SO and FO
	Thermal by convection	JO and FO
	Thermal through an impermeable surface	FO and FO
	Hydraulic and thermal by a permeable surface	FO and FO

to which should be added the electric contact between strand components discussed in section 2.3.1.

2.4.4 Coupling of equation and final PDEs set

Up to this point, the equations modeling the fluid and solid components have been described separately. However, due to the connections seen in paragraph 2.4.3, the thermohydraulic equations must be solved as a single set of PDEs. The number of equations in the system increases in proportion to the level of detail used to discretize the conductor into its basic components, following this relationship:

$$N_{eq} = 3N_{ch} + N_{st} + N_{jk} \qquad (2.4 - 5)$$

Once the coupling of the equations is defined, it is useful to rewrite them in a matrix form for easier handling. For this purpose, some notation should be introduced: $\boldsymbol{u}$ and $\boldsymbol{s}$ represents the unknowns and source vectors, respectively, while $\boldsymbol{\mathcal{M}}$, $\boldsymbol{\mathcal{A}}$, $\boldsymbol{\mathcal{K}}$, and $\boldsymbol{S}$ are the square matrices of coefficients. Their general definitions can be found in [46]. The elements of the last matrix, $\boldsymbol{S}$, originate from the right-

hand side of the PDEs, as there are terms that include the unknowns. Therefore $\boldsymbol{s}$ is constructed only from the Joule and external linear power sources of the solid components. The matrix form of the set is:

$$\mathcal{M}\frac{\partial \boldsymbol{u}}{\partial t} + \mathcal{A}\frac{\partial \boldsymbol{u}}{\partial x} + \frac{\partial}{\partial x}\left(\mathcal{K}\frac{\partial \boldsymbol{u}}{\partial x}\right) + \mathcal{S}\boldsymbol{u} = \boldsymbol{s} \qquad (2.4\text{ - }6)$$

This set cannot be classified according to the typical PDE classifications since it combines both hyperbolic and parabolic features.

Equations (2.4 - 6) represents the matrix form of a coupled, non-linear system of partial differential equations (PDEs) that are first-order in time and second-order in space. Given the impracticality of finding an analytical solution to this system, a numerical approach is employed to solve the problem. For spatial discretization, the Finite Element Method (FEM) has been chosen. Time discretization is carried out using an implicit method (such as Backward Euler or Crank-Nicolson) due to the stiffness of the problem. Implicit methods are generally preferred over explicit ones because they offer better stability properties.

2.5 Coupling electrical and thermohydraulic models

In this section we will explore the close relationship between the electrical model and the thermal-hydraulic model that the code seeks to preserve. As stated in section 2.3.2, the electrical resistivity of materials is a function of temperature, which in turn is a function of the amount of heat deposited on the current carrier by the Joule effect. The thermal-hydraulic and the electric problems are hence coupled. The whole problem (thermal-hydraulic plus electric) is formulated with two nested loops: the outer one dealing with the solution of the thermal-hydraulic problem for the whole conductor and the inner one dealing with the electric problem for all the current carriers that constitute the conductor.

After a suitable initialization, for each thermal-hydraulic time step (outer loop), a defined number of electric time steps (inner loop) are carried out to solve equation $2.3 - 11$ assuming that the temperature is constant to simplify the problem. The last electric time step brings the electric time to the next thermal hydraulic time step. In this transient, current, voltage and electric resistance of SC materials are updated and combined to compute the Joule power deposited on the various current carriers. This is added as an inner contribution to the heat sources that appears in equation $2.4 - 3$ ($Q_{Str,Joule}$) that are solved to update all the thermal-hydraulic variables, including the temperature of strand objects.

With the newly evaluated temperature a new set of electric time steps is carried out to compute current, voltage and electric resistance used to update the source terms of equation $2.4 - 3$ and so on.

This coupling structure of the problem, summarized in Figure $2.5 - 1$ is subordinate to the difference between the time scales of the electric problem which is orders of magnitude lower than the time scale of the thermal-hydraulic problem.
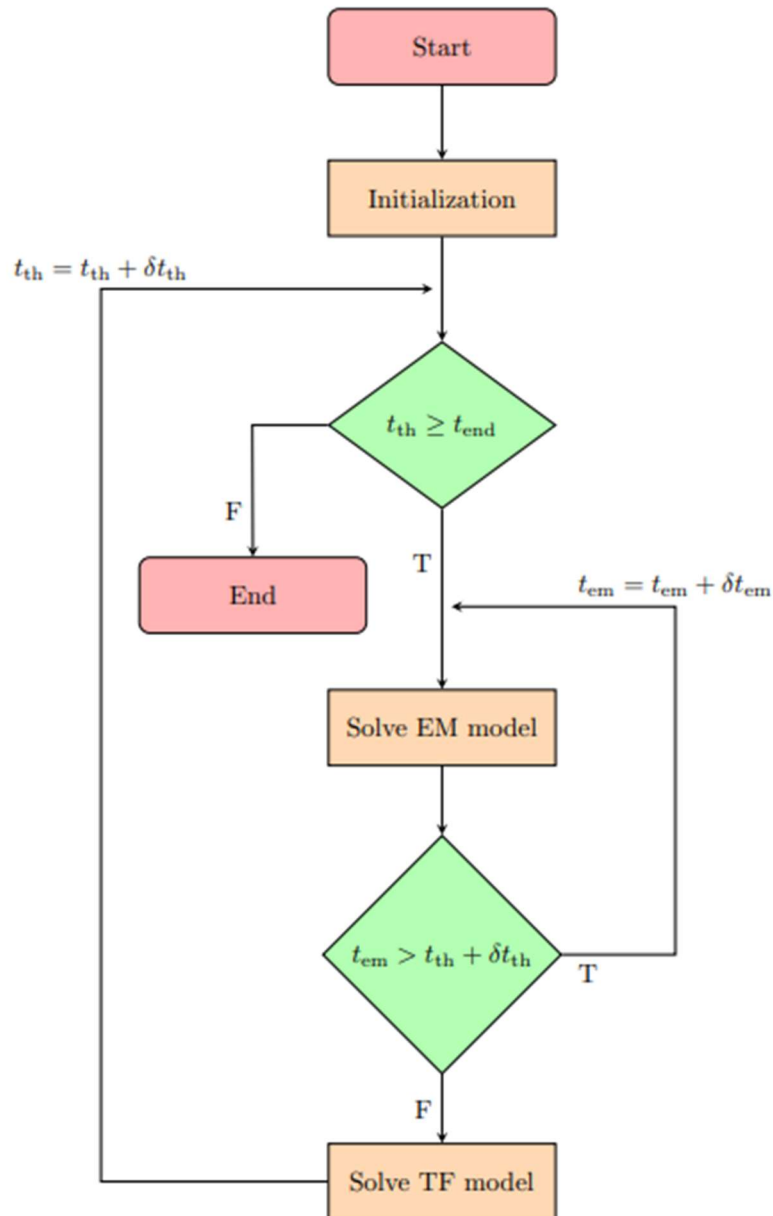

Figure 2.5 – 1: Representation of the coupling that exists between the electrical model and the thermal model. Two loops can be seen within the flowchart, one relating to the electrical model and thermal source construction, and one relating to cable resolution, which also involves the thermohydraulic model.

3 Case study and results

In this chapter, the results of the experiments conducted for the validation and verification of the recently implemented electrical model will be presented. The main objective is to ensure that the model functions correctly both on its own and once coupled with the thermohydraulic model.

To achieve this goal, a benchmark was performed between the OpenSC^2 software and a transient simulated in 4C. This comparison is essential to verify the accuracy and reliability of the electrical model, as well as its effective integration with the thermohydraulic model. The obtained results will provide a solid evidence base to confirm the model's validity and its applicability in realistic scenarios.

Section 3.1 will present the main input data characterizing the cable geometry, materials, type of transient studied, and the boundary conditions used.

Section 3.2 will describe the choices made to input this data into OpenSC^2 to replicate the same transient, including geometric choices and evaluation of heat exchange parameters.

Section 3.3 will cover the verification of the solution, with a study of spatial and time convergence.

Finally, Section 3.4 will present the benchmark results and compare them with the reference results, followed by a critical analysis of the findings.

3.1 Presentation of the case study

The study [40] examines quench propagation in an ENEA HTS cable-in-conduit conductor designed for fusion applications, specifically for an insert in the central solenoid of the Italian Divertor Tokamak Test (DTT) facility [47]. The study particularly wants to analyze the temperature peak, which should be compared with a suitable design criterion, and then parametrically is evaluated the effects of delay and rapid current-discharge times on the conductor's peak temperature, to prevent damage to the HTS.

The ENEA HTS CICC is extensively described in the reference, and the main information is summarized here. It features an aluminum core with six twisted slots, each with a twist pitch of 0.5 meters. Each slot measures 4.3 x 4.3 mm and contains 20 non-soldered REBCO tapes, each 4 mm wide, secured in place by an aluminum filler (see Figure 3.1 – 1). The entire cable is enclosed within

a 1.5 mm thick aluminum pipe. It is 132 m long, with an external diameter of 25 mm. Twelve side channels, each approximately 0.15 mm wide, and one central channel with a diameter of 5mm can be identified.

This conductor will be cooled with a mass flow rate of ~ 5g/s of supercritical helium (SHe) at an inlet pressure of 6 bar and a temperature of 4.5 K. These thermodynamic conditions are chosen primarily to allow the coil to connect to the same cryo-distribution system as the LTS magnets [40], and also to provide a significant temperature margin to prevent quenching of the superconducting tapes.

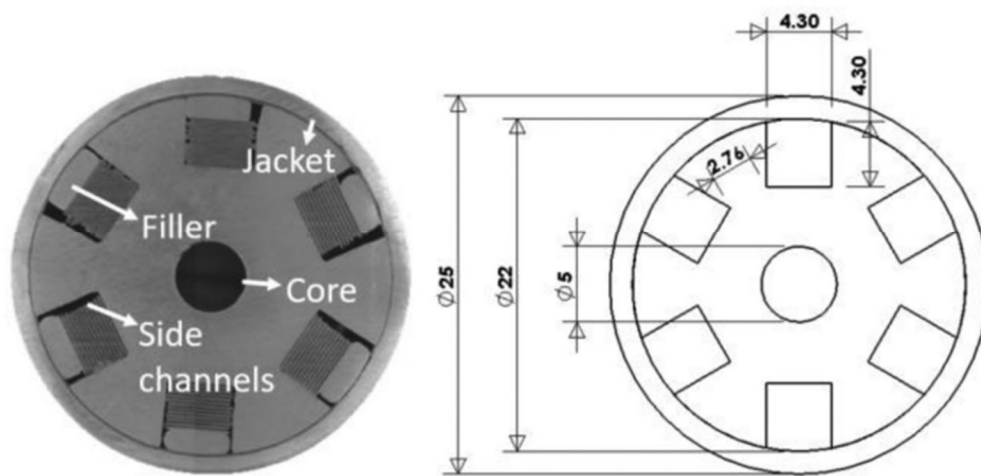*Figure 3.1 - 1: ENEA HTC CICC cross section and relevant geometrical information, adapted from* [40] .

The driver of the transient is a 0.1 s long heat pulse (from 0.01 s to 0.11 s), deposited axially on 10 cm in the central part of the conductor, in all the Stacks. The total energy deposited to induce the quench is 150 J. Making the calculation 150 J are equal to 2500 W/m of linear heat applied on each Stack (Figure 3.1 – 2):
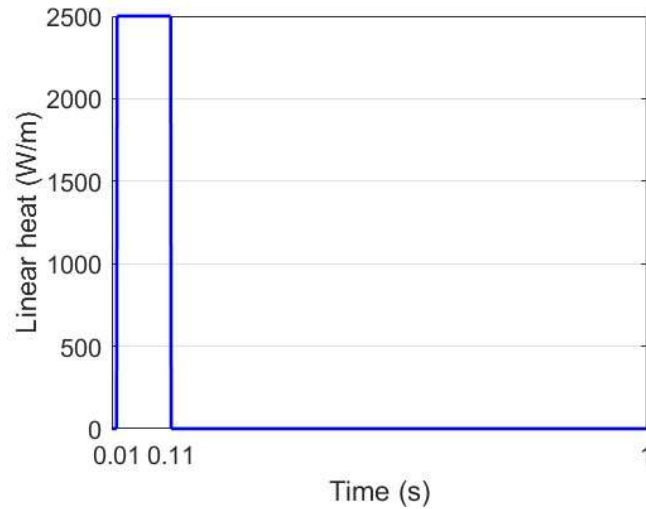
Figure 3.1 – 2: Linear heat deposited in each stack from 0.01s to 0.11 s.

The temperature increase due to the heating of the Stacks is intended to initiate the quench of the cable, which will transition from a superconductive state to a normal state. This transition results in a significant increase in the electrical resistance of the SC materials, and for this reason, the currents will tend to redistribute along the cross-section of the cable. The non-SC materials that make up the cable, carrying current, will dissipate current in the form of heat due to the Joule effect, causing a further increase in temperature. For this reason, once the quench is detected, the total current of 32 kA is discharged to maintain the integrity of the cable and limit the temperature peaks reached within the stack. The reference assumes a quench detection time for the cable at t_det = 0.4 s, and a delay before discharge of t_del = 0.25 s. OpenSC^2 does not yet have a quench detection mechanism among its functionalities, so the discharge timing of t_dis = 0.65 s will be adhered to. The current inside the table can be written as:

$$\begin{cases} I(t) = I_0 & if\ t < 0.65\ s \\ I(t) = I_0 e^{-t/tau} & if\ t \geq 0.65\ s \end{cases} \qquad (3.1-1)$$

In Equation 3.1 – 1 I_0 is the initial current in each stack, t is the time and tau is the current discharge time, for this calculus set to 0.5 s. The discharge characteristic can be seen in Figure 3.1 – 3:
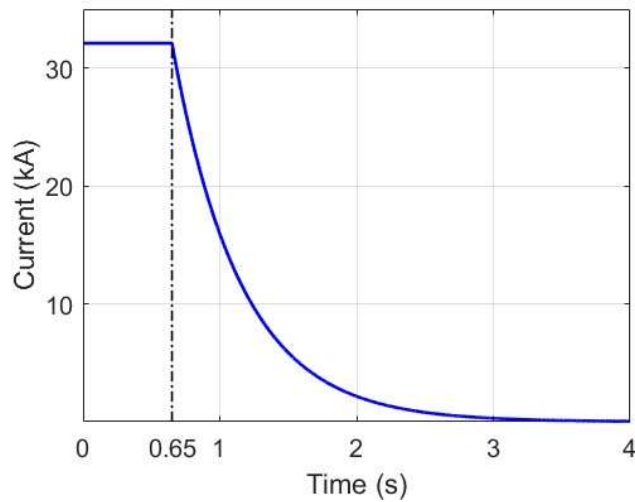
Figure 3.1 – 3: Current discharge inside the cable after t=0.65 s.

For this analysis, Dirichlet boundary conditions are applied to the fluid, with an inlet pressure of 6 bar, an inlet temperature of 4.5 K, and an outlet pressure of 5 bar. The solid has boundary conditions with an inlet and outlet temperature of 4.5 K, and the cable is considered adiabatic.

The magnetic field is fixed at 17 T for the entire duration of the transient, while the current initially has a value of 32.1 kA and varies according to the power law described in equation 3.1 – 1.

After consulting with industry experts, the starting point of the heating was set at 49.5 meters and the endpoint at 50.5 meters.

To electrically solve the problem, the electric potential at the last node was set to zero.

A summary of the most relevant geometrical and operational parameters that characterize the case study is presented in Table 3.1 -1:

Table 3.1 - 1: Summary of the most relevant geometrical and operational parameters of the case study.

Parameter	Value	Units
Length	132	m
Initial current	32.1	kA
Magnetic field	17	T
Inlet/outlet pressure	6/5	bar
Inlet temperature	4.5	K
Total mass flow rate	~5	g/s
Voltage at conductor end	0	V
Current discharge time constant	0.5	s
Time when heat pulse start	0.01	s
Time when heat pulse end	0.11	s
Linear heat in each Stack	2500	W/m
Point in which the heat start	49.5	m
Point in which the heat end	50.5	m
Time when current is dumped (s)	0.65	s

3.2 Discretization of the problem with OpenSC^2

To reproduce the case study in Section 3.1, it was useful to analyse the geometry of the system and the transient before moving forward with the simulations. This step is described in Section 3.2.1.

Subsequently, the thermal and electrical interfaces of the system were examined, and their critical values were quantified. This will be explained in Section 3.2.2.

Finally, it was necessary to evaluate the values to be inserted into the Stack class for the composition of the HTS tape, to allow the discretization of the superconductive component of the cable, and the evaluations made are described in Section 3.2.3.

3.2.1 Geometry of the cable

Considering the section shown in Figure 3.1 – 1, each stack, channel, or any other component of the cable can be regarded by OpenSC^2 as an individual object, to be coupled with others from an electrical-thermal-hydraulic perspective. The aluminum core, according to this approach, could be treated as a single object. However, based on a convergence study [40] comparing peak temperatures

of the stack with the number of regions into which the aluminum core object is divided, the ideal number of objects to consider is 18. This provides a balanced compromise between the number of objects analysed and the peak temperatures measured within the stack.

Following this convergence study and to overlap as closely as possible to [40], the cable section has been discretized accordingly, as depicted in the Figure 3.2 – 1:
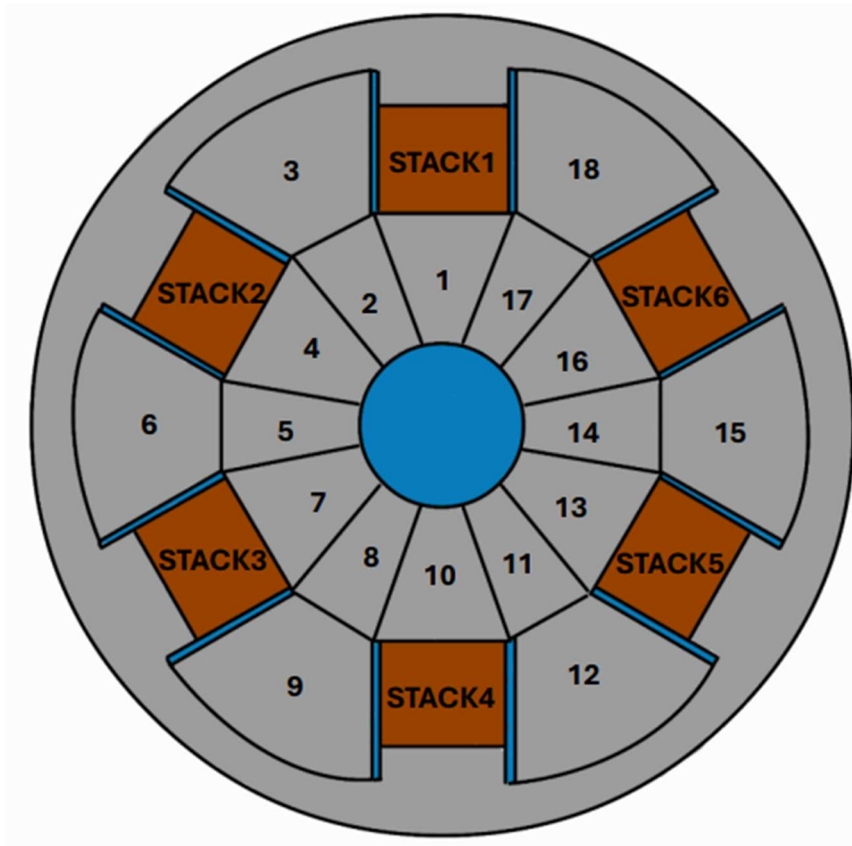
Figure 3.2 – 1: section of the cable with all the subregions. In orange the objects Stack, in blue the objects channel and in grey the aluminium regions.

Also, the jacket can be managed in many ways, but since it is not the focus of this analysis, it will be modeled with a single component.

Considering how the problem would have been studied in OpenSC^2, there would have been 6 Stack objects, 18 Stabilizer objects, 13 channel objects (12 side channels and one central channel), and 1 Jacket object, for a total of 38 objects.

Carefully analyzing the geometry of the section and the type of transient to be studied, some important simplifications can be made to save computational power.

Referring to the section of the cable shown in Figure 3.1 – 1, it can be argued that the cable is axisymmetric. Based on this information, the minimal computational domain of the section of the cable is the one subtended to an angle of 30°, which corresponds to 1/12 of the cable.

About the initial conditions, the parameters are uniform across the entire surface of the cable. The inlet and outlet pressures of the channels are fixed beyond the channel, as well as the inlet temperature. All solids are initialized at the same temperature, and assuming the cable is in a superconductive state at the beginning of the transient, the current will be evenly distributed among all six stacks.

Regarding the thermal transient, it is stated that each Stack is heated equally to initiate the transient, with a total of 150 J applied to the cable. Since the heating is uniform across all the Stacks, and the external heating represents the trigger of the quench to be analysed, it could be significantly beneficial to model only one half of the six Stacks that make up the cable.

Given the considerations, the cable has been simplified as shown in Figure 3.2-2:
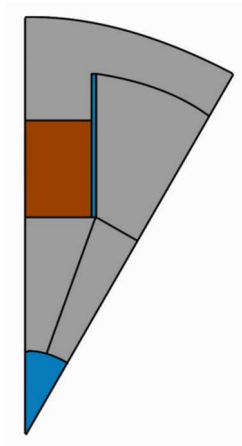
Figure 3.1 - 2: Section of the cable considered for the analysis.

Thanks to this consideration, it is possible to significantly reduce the computational domain of the problem as shown in Figure 3.2 – 3 that introduce also the nomenclature of the conductor components. In the end from a total of 38 conductor components modelling the whole cable, the minimum set of components considered in the remainder of this work is 7, namely 1 Stack object, 3 Stabilizer objects, 2 Channel objects (1 side channel and 1 central channel), and 1 Jacket object. The reduction in computational cost is even more evident if the number of equations solved per each node is considered: each node of the whole cable is modelled by 64 thermal hydraulic equations and 48

electric equations while the selected discretization is characterized by 11 thermal hydraulic and 8 electric equations.
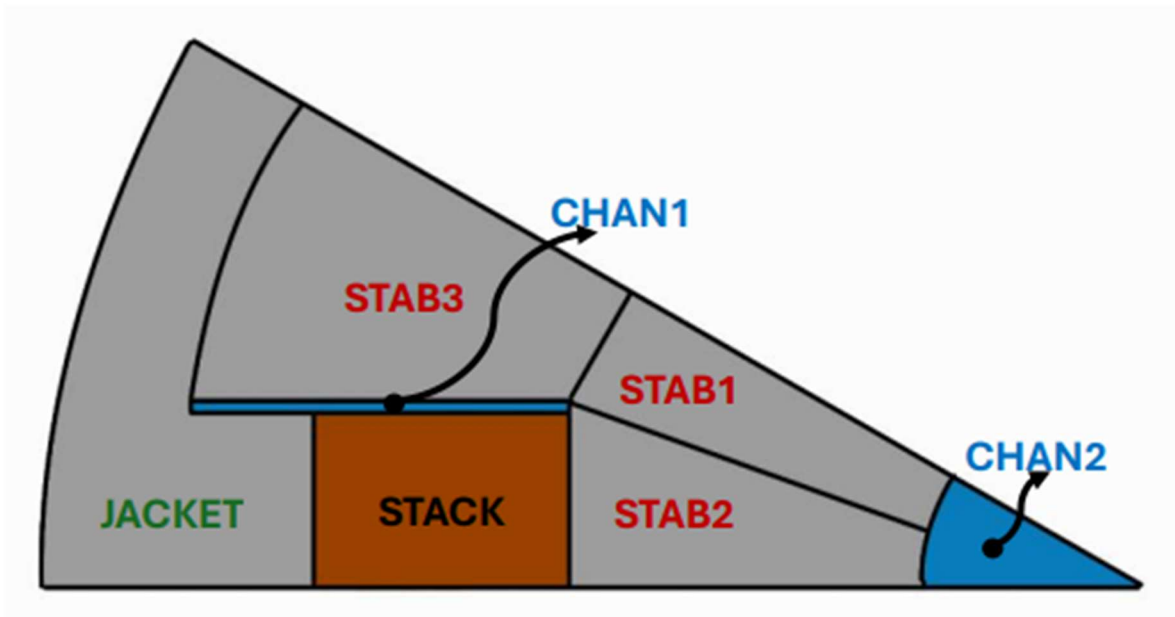
Figure 3.2 - 3: Cross section of the cable considered for the calculation with OpenSC². The plate colors for each name are to be considered consistent with the discretization performed according to the software, as shown in Table 2.2 - 1.

Each of these 7 objects was discretized according to the data prescribed in Table 3.1-1, taking care to scale to 1/12 the energy applied to initiate the quench, as well as the total current carried by the cable. So the liner heating applied and the nominal current used in the simulation are respectively 1250 W/m and 2675 A. The input file used for the calculation are collected in Appendix A.

3.2.2 Thermal-hydraulic and electrical interfaces

Following the choice of the simplified cross-section, the types of thermal interfaces present between the components of the problem were analysed (Figure 3.2 – 4).

As seen in Table 2.4-1, OpenSC² provides various connections to couple the cable objects.

The Stack is coupled by conduction to the aluminum Jacket and to the subregion in the centre of the cable, also made of aluminum, called "Stab 2"; the latter is coupled by conduction to "Stab 1", which in turn is coupled to "Stab 3".
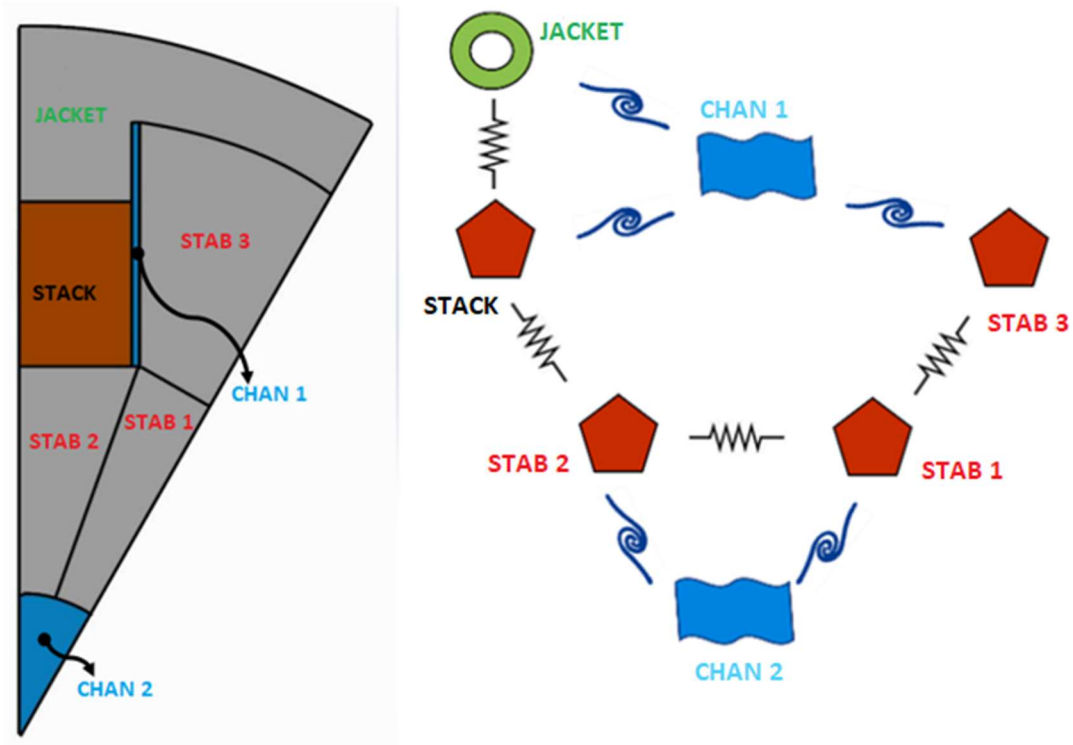
Figure 3.2 - 4: Thermal interfaces between the objects of the discretized cable. The symbols of the objects and the type of connection are adapted from [42].

Regarding the parameters inserted for the thermal couplings, OpenSC^2 has already implemented the correlations of the transport coefficient for the channels as shown in Table 3.2 – 1

Table 3.2 – 1: Transport coefficient correlations for the channels.

Channel	Nusselt number	Friction factor
CHAN 1	$0.42 \cdot Re^{0.71}$	$2.21 \cdot Re^{-0.4} (Re > 10^4)$
CHAN 2	$0.023 \cdot Re^{0.8} \cdot Pr^{0.4}$	$\frac{1}{\sqrt{f}} = -2log_{10} \left(\frac{\varepsilon}{3.7 D_h} + \frac{2.51}{Re\sqrt{f}} \right)$

For thermal exchange between solids, the guidelines given in [40] were followed. Therefore, for the contacts between "Stack" and aluminum ("Jacket" and "Stab 2"), between "Jacket" and "Stab 3", and between Stab element, reference can be made to the values in Table 3.2-1. Specifically, for the contact between aluminum and copper, two values were present, and the highest value was chosen, to ensure maximum heat dissipation. The difference between the value indicated in the Table 3.2 – 2 and the other value that were present in [48] does not significantly affect the peak temperature reached by the

stack. In fact, simulating the same configuration with the minimum value ($42\,000\;W/(m^2 \cdot K)$) instead of $56\,000\;W/(m^2 \cdot K)$) results in a difference of about 1 K.

The calculation for the for the thermal conductance between "Stab 2" and "Stab 1" and between "Stab 1" and "Stab 3" was performed as prescribed in [40]: the thermal contact resistance was evaluated as $\delta/k_{aluminium}$, assuming a contact surface thickness δ of $0.1\;mm$.

Table 3.2 – 2: Thermal contact conductances

Material	h_c $W/m^2 \cdot K$
"Jacket" – "Stab 3"	11 400
"Stack" – "Stab" or "Jacket"	56 000
"Stab" – "Stab"	17 000

Finally, the electrical couplings were evaluated. It should be remembered that, at time being, in OpenSC^2 only the Strand Object is allowed to carry a current, as already mentioned in Chapter 2.

The scheme of the electrical connections will therefore be as shown in Figure 3.2 – 5; note that the jacket is not included.
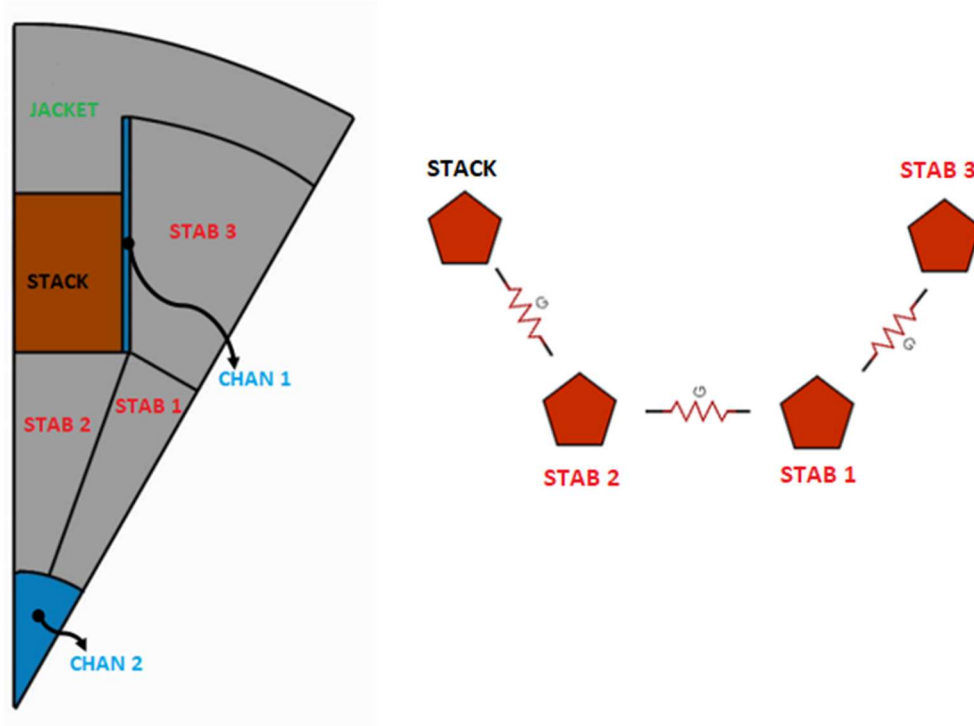
Figure 3.2 – 5: Electrical interfaces between the objects of the discretized cable. The symbols of the objects are adapted from [42].

Also in this case, values mentioned in [40] are used to fill the conductance matrix. For the contact between "Stack" and "Stab 2", the electrical resistance was directly indicated, while for the contact between the core subregions, a very high electrical conductance was assumed. The values entered as input into OpenSC^2 are described in Table 3.2 – 3:

Table 3.2 – 3: Transverse electrical conductances between Strand Objects

Connection	G S/m
Stack - Stab 2	$3.33 \cdot 10^3$
Stab 2 - Stab 1	$1 \cdot 10^{12}$
Stab 1 - Stab 3	$1 \cdot 10^{12}$

For the contact perimeters of heat exchangers and other geometric data of the system, please refer to the data present in the tables of Appendix A.

3.2.3 Tape topology

In OpenSC^2, it is necessary to define in detail the composition of the Stack Object, with parameters such as the number of tapes that make it up, the materials of which it is composed of and the volume per unit length occupied by each material. These details were not available in [ref] and there is neither an explicit nor implicit reference to a tape design, so the choice of tape was based on the previous ENEA cable model [49] with only five slots for the Stacks, using SCS4050 tapes produced by Superpower [50]. These tapes have a configuration as shown in Figure 3.2 – 6.
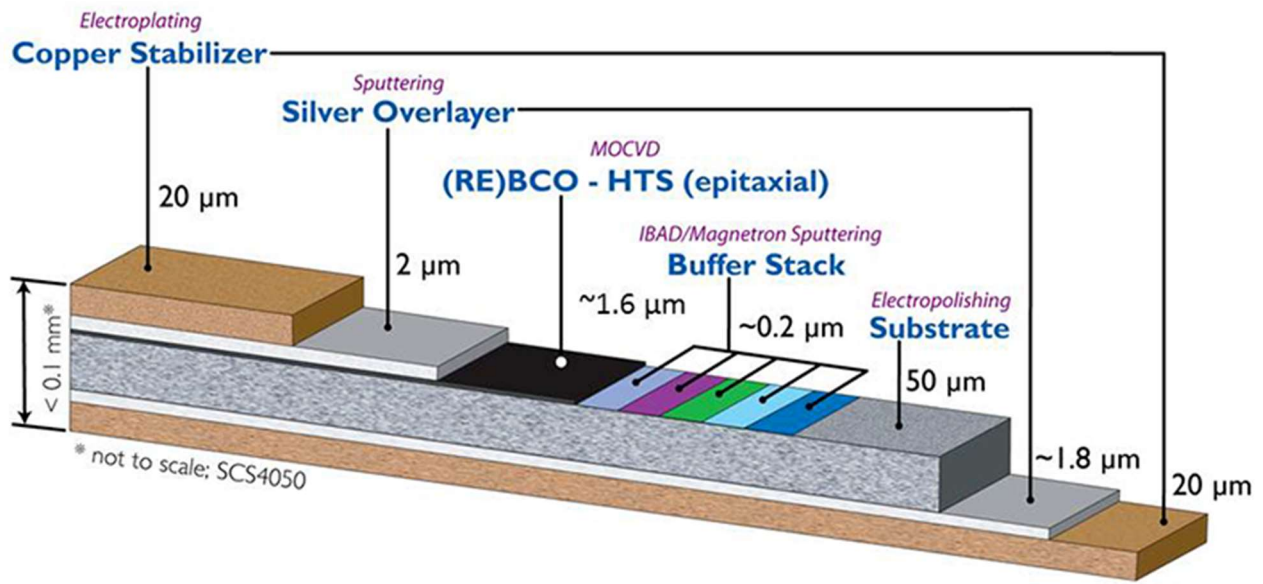
Figure 3.2 – 6: Composition of the tape SCS4050 by Superpower [50]

In [40], 20 tapes were specified, but with the chosen configuration, it was not possible to insert an integer multiple of the SCS4050 tape into the slot provided for the stack of tapes.

Since the Stack class in OpenSC^2 internally homogenizes the object and its materials (see Appendix B4), it was decided to address the issue of the mismatch between the tape thickness and the intended space occupied by the stack by performing a preliminary reshaping of the tape. Considering the measurements of the SCS4050 by Superpower, the ratios between the thickness of each material and the total thickness of the tape were calculated. This ratio was then multiplied by the total height occupied by the Stack, as defined by the geometry, resulting in a new single tape (Table 3.2 – 4).

Regarding the buffer, it has been neglected in this analysis because generally its thickness is orders of magnitude smaller than all other materials, and also because the properties of the buffer have not yet been implemented in OpenSC^2.

Table 3.2 – 4: Reshaping of the superconducting tape used.

Material	Thickness (m)	Ratio	Thickness after reshaping (m)
Copper	$4 \cdot 10^{-5}$	1.68%	$4.9 \cdot 10^{-5}$
Hastelloy	$5 \cdot 10^{-5}$	52.41 %	$1.530 \cdot 10^{-3}$
Silver	$3.8 \cdot 10^{-6}$	41.93 %	$1.224 \cdot 10^{-3}$
HTS REBCO	$1.6 \cdot 10^{-6}$	3.98 %	$1.16 \cdot 10^{-4}$
Total	$9.54 \cdot 10^{-5}$	100.00 %	$2.92 \cdot 10^{-3}$

3.3 Solution Verification

Up to this point all the necessary input data were exhaustively discussed. This section discusses the criterion on which the spatial discretization pitch Δx and the time step Δt are selected. This allows also to make some considerations on solution verification.

Studying convergence in time and space provides critical assurance of the quality and reliability of the results obtained from numerical simulations, ensuring that the model is well-defined, accurate, and representative of the studied physical phenomenon.

To limit computational costs associated with this operation, it was chosen to verify the solution only over the meter of cable containing the heated zone to initiate quench, specifically the segment between 49.5 m and 50.5 m.

3.3.1 Space Convergence

For the space convergence analysis, in order to limit computational effort, only a one-meter length of the cable was studied. This length was chosen so that the applied heating is positioned exactly in the middle of the cable.

Specifically, the one-meter length of the cable studied will be the section between the coordinate x1 = 49.5 m and the coordinate x2 = 50.5 m. Once the one-meter length of the cable was selected, an initial thermohydraulic simulation of the cable was conducted to evaluate the conditions of the fluid and the solid at coordinates x1 and x2 under steady-state conditions. The parameters read at x1 and x2 were used as Dirichlet boundary conditions for the space convergence analysis and are represented in Table 3.3 – 1.

Table 3.3 – 1: Boundary conditions imposed to the cable for the study in the space convergence

Parameter	Value	Units
Inlet mass flow CHAN 1	$2.40 \cdot 10^{-5}$	g/s
Inlet mass flow CHAN 2	$4.14 \cdot 10^{-4}$	g/s
Inlet temperature for the channels	4.5	K
Outlet pressure for the channels	$5.62 \cdot 10^{5}$	Pa
Inlet/outlet temperature for the solids	4.5	K

Then, on the Stack component, a linear thermal power of 50 W/m was applied along the entire length of the cable. A sufficiently long transient time of 20 s was studied to ensure the cable reached thermal equilibrium. To assess the quality of the mesh, the steady state temperature of the Stack at the end of the cable segment, i.e. the hot spot, was considered. The cable length is uniformly discretised by progressively reducing the Δx between nodes so that the mesh of each simulation is finer than the mesh of the previous one. The selected values for Δx are 10 mm, 5 mm, 2 mm, 1 mm, 0.5 mm, 0.2 mm and 0.1 mm.

It should be noted that the electrical model is not involved in this study since the equations do not include spatial derivatives (lumped parameter model).

It was observed that as the mesh was refined, temperatures gradually decreased. It is reported in Figure 3.3 - 1 the engineering convergence study.
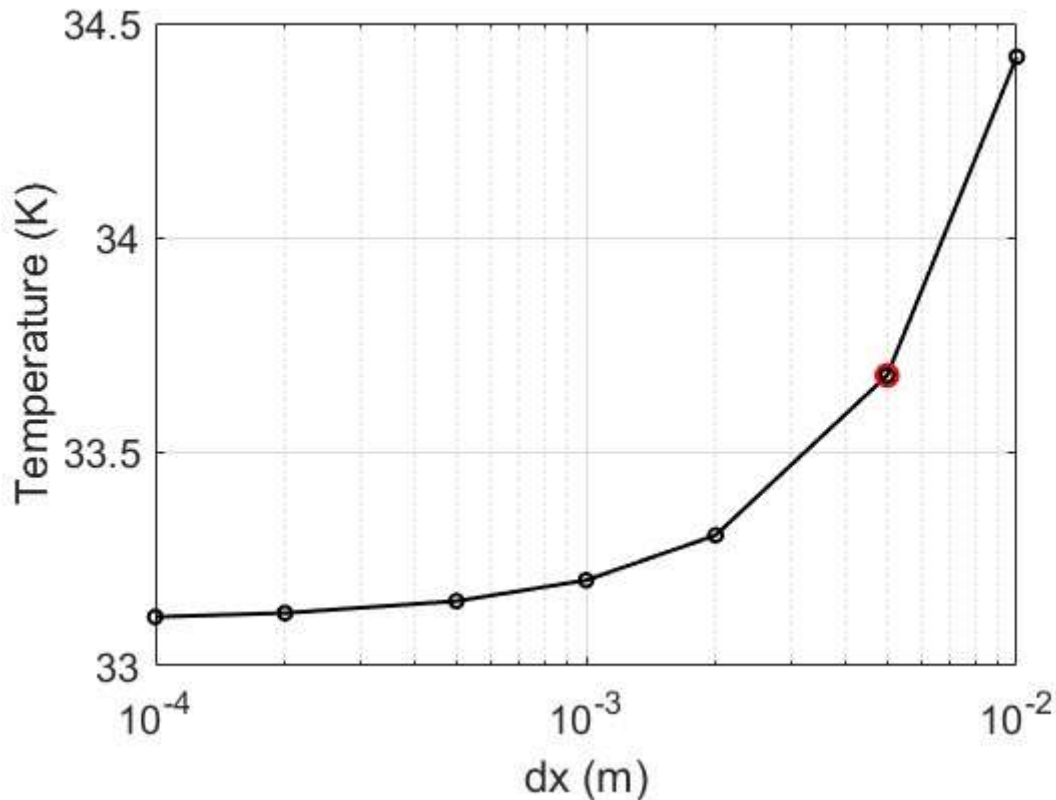
Figure 3.3 – 1: Engineering space convergence plot of Stack temperature. In red is selected dx = 5mm, the chosen space grind for the calculation.

The independence of the solution from the spatial discretization parameter appears to be achieved with a very refined mesh, on the order of 0.1 mm.

However, this value is impractical for simulations because once the electrical model is included, the computational cost becomes excessively high. Assuming a dx = 0.1mm on a cable of 1 m would mean having 10'000 elements, which offers significant temperature accuracy gains but is computationally unsustainable. Adding the current into the system further exacerbates this issue, making program execution extremely slow and memory intensive. Trying to make this kind of simulation fter waiting 10 minutes for a time step a memory error was encountered.

For this reason, a much coarser mesh was chosen, despite the potential error that may result from this choice. The chosen Δx for the simulations will be 5 mm.

3.3.2 Time convergence

In the time convergence analysis, the accuracy with which time-dependent variables are calculated is evaluated. For this reason, it is important to include the electrical model, whose time dependency is

clearly visible in Equation 2.3 - 11. The imposed transient will therefore be on the one-meter cable already studied during the space convergence, with the space grid chosen of 5 mm and with the same boundary conditions as in Table 3.3 – 1, but this time with the thermal pulse of Figure 3.1 - 2 multiplied by a scale factor of 0.5 (only half of the Stack is considered for geometric reasons discussed in Section 3.2) with an initial heating coordinate of x = 0.45 m and a final coordinate of x = 0.55 m. A total current of 2675 A was initialized, which is 1/12 of the total current (refer to the symmetry conditions in Section 3.2). The discharge of the current is set to start at t = 0.65 s (Equation 3.1 - 1), and the transient was stopped at t = 0.70 s. An interval of 0.05 s is considered sufficient to evaluate the accuracy of the time derivatives of the system based on the chosen time step width. The time steps studied were dt = 10 ms, dt = 5 ms, dt = 2ms, dt = 1ms, dt = 0.5ms and dt = 0.1 ms. At the end of the transient, the temperature and current of the Stack at the coordinate x = 0.5 m (the point located at the center of the heating, which is expected to have the greatest variations in temperature and therefore current) were considered.

The results of the engineering time convergence study are shown in Figure 3.3 – 2.

The independence of the solution from the time step, both for temperature and the current, were achieved at t = 0.1 ms.
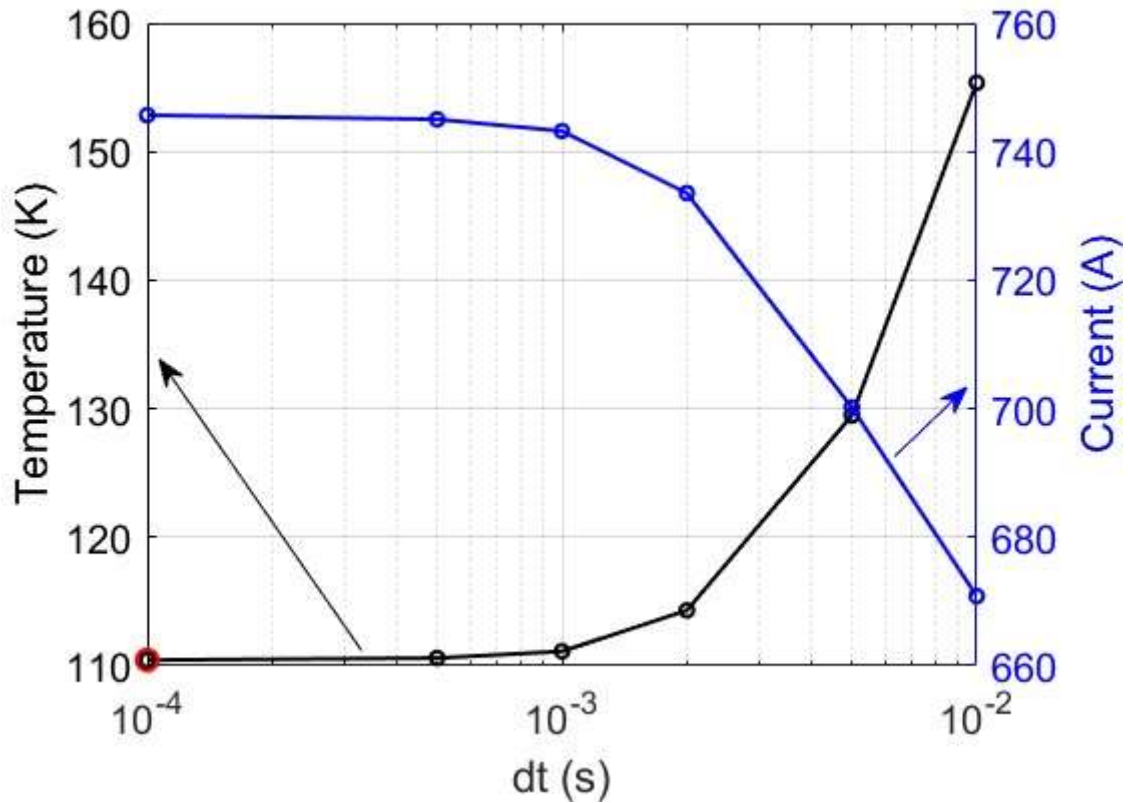
Figure 3.3 – 2: Engineering time convergence plot of Stack temperature on the left y-axis (black) and of Stack current on the right y-axis (blue). In red is selected dt = 0.1ms, the chosen time step for the calculation.

In this case, the time step of the case study was prescribed by [40], varying between 1 ms and 0.1 ms. As observed from the study of time convergence, this range appears to yield the best results. The selected value of the minimum time step for the following analysis is 0.1 ms.

From Figure 3.3 – 2, one can also appreciate an initial experimental indication of the transient: higher temperatures are associated with lower currents, and vice versa. This is the best outcome that could be expected, as it is important to remember that the electrical properties of materials depend on their temperatures. Higher temperatures result in higher levels of electrical resistance, and consequently, less current is able to flow.

3.4 Benchmark results

In this section, the results obtained are presented on the base of the considerations and analysis carried out in sections 3.1, 3.2 and 3.3 throughout Chapter 3 up to this point. It is organized as follows.

Section 3.4.1 clarify what grid has been chosen in light of verifying the solution for the entire length of the cable.

Section 3.4.2 is dedicated to current redistribution and how the electrical model of OpenSC^2 can track the time evolution of current within the components that make up the cable.

Section 3.4.3 presents the benchmark of the OpenSC^2 model against the 4C code. Temperature comparison as well as the role of the current redistribution on the hot spot in the Stack component are discussed.

3.4.1 Grid Selection

For the simulation presented, compromises had to be made between the selection of the spatial discretization pitch, the time step and the computational cost required for the simulation. Specifically, two OpenSC^2 features were exploited, namely a locally refined spatial mesh and an adaptive time step.

As for the spatial discretization, a region of one meter length around the heated region (from x = 49.5 m to x = 50.5 m) is refined with a 5 mm spatial discretization pitch, since the peak temperature is expected to occur precisely at the midpoint of the heating. Outside this region, the spatial discretization parameter gradually increases up to a maximum of 68.5 cm to the left of the region and up to 54.8 cm to the right of the region. The selected value for the Δx in the refined region comes from a space convergence study (see section 3.3.1). A representation of the locally refined mesh is shown in Figure 3.4 – 1.

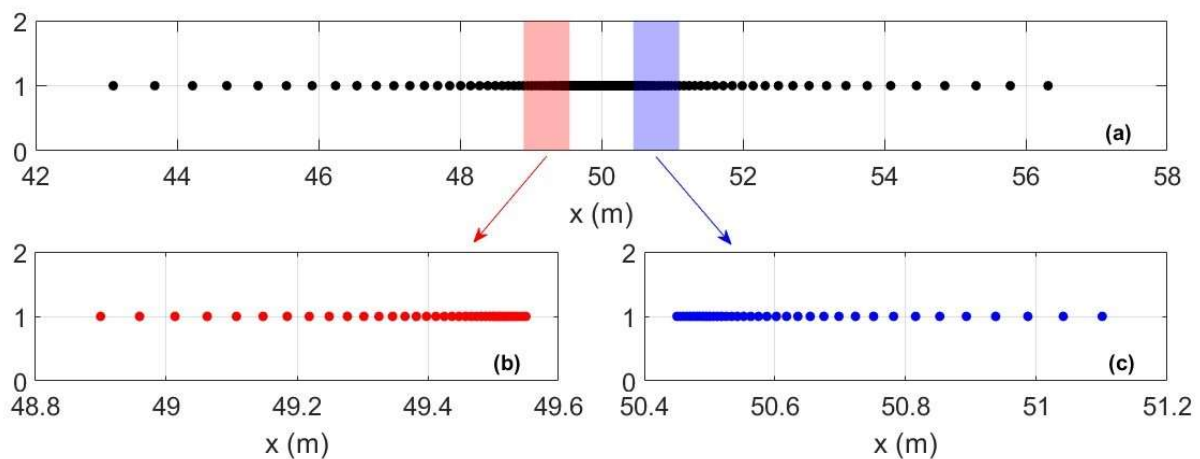*Figure 3.4 – 1: Representation of the locally refined mesh. One refined region that goes from x = 49.5 m to x = 50.5 m and two coarse regions. a) zoom of the increase ratio that permits the transition from the refined region to the coarse regions. b) zoom of the smooth transition from coarse left to refined region. c) zoom of the smooth transition from refined region to the coarse right.*

Regarding time, an adaptive time step was used with a minimum step of 0.1 ms and a maximum step of 10 ms. This implies a transition to a much more relaxed time step after major transients occurred (such as the heat pulse, occurring from 0.01 s to 0.11 s, and the dumping of current starting at 0.65 s). The upper and lower bounds of the adaptive time step are given in [40] and are confirmed by a time convergence analysis (see section 3.3.2).

3.4.2 Current Analysis

In the simulation, the heating is intended to disturb the initial superconducting conditions. At the beginning of the simulation the current will be carried entirely by the Stack, and since it is in superconductive regime this has no effect on the temperature of the cable. Then the heating process increase the temperature Stack, and the transient begins. Once the HTS reaches the current sharing temperature, the Stack should begin redistributing current to the other current carriers, following the current divider principle as explained in Section 2.3.1. Therefore, what is expected to be observed following heating is a gradual reduction of current in the Stack and an increase of current in the aluminum components of the core. This theoretical behavior is confirmed by the current time evolution shown in Figure 3.4 – 2, where in the upper figure is also represented the temperature evolution of the Stack.
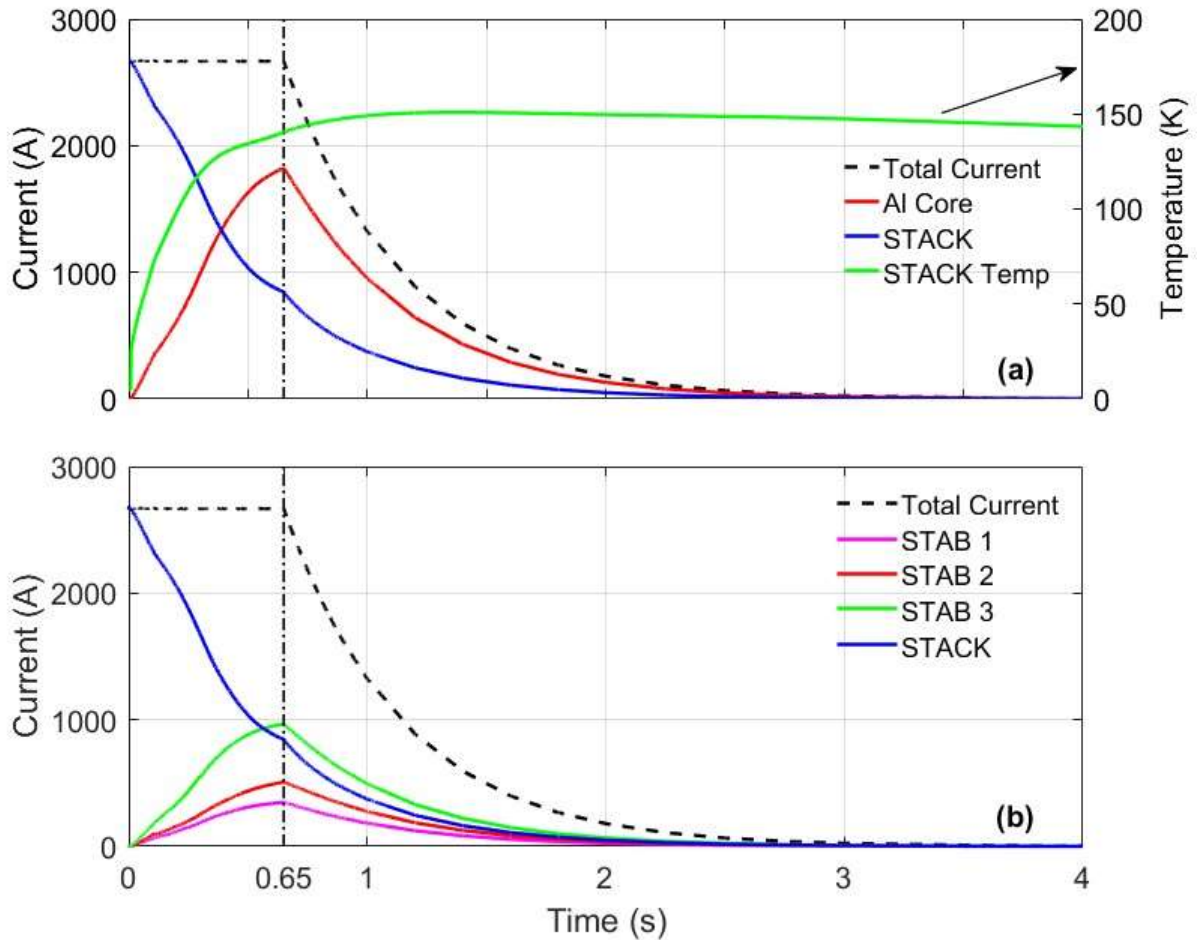
Figure 3.4 – 2: Graph showing the current trend over time at the coordinate x = 50 m (midway through heating). a) current distributed between the Stack and the aluminum core. In green is represented also the Stack temperature; b) a detailed breakdown in the three subregions of the aluminum core. The vertical dashed black line represents the current damping set at t=0.65 s.

The currents are distributed among the various components according to the predictions of the electrical model.

Despite the electrical conductivity being nearly negligible between the aluminum regions, it is interesting to observe how different currents are still carried. This is understandable considering the different cross-sectional areas between the regions, which, as seen in Equation 2.3 - 13, at constant electrical resistivity (a function of temperature), significantly affect the calculation of resistances.

A numerical proof of this fact can be seen in x = 50.0 m and t = 0.65 s in Table 3.4 – 1.

Table 3.4 – 1: Electrical resistivity versus electrical resistivity divided by the cross section of each object Stab, at coordinate x = 50.0 m and time t = 0.65 s.

Object	ρ_{el} [$\Omega \cdot m$]	ρ_{el}/A_{Stab} [Ω / m]
Stab 1	$1.479 \cdot 10^{-8}$	$3.749 \cdot 10^{-3}$
Stab 2	$1.536 \cdot 10^{-8}$	$2.510 \cdot 10^{-3}$
Stab 3	$1.411 \cdot 10^{-8}$	$1.340 \cdot 10^{-3}$

3.4.3 Benchmark against 4C code

In this section, the temperature time evolutions for the components comprising the cable are presented.

Figure 3.4 – 3 shows the results obtained in the case study discussed in [40] with the 4C code, with a temperature peak of $\sim 130\ K \pm 20K$ for the Stack, and a difference in temperature between HTS regions and the aluminum regions that can reach the 50 K in the first 0.5 s of simulation:
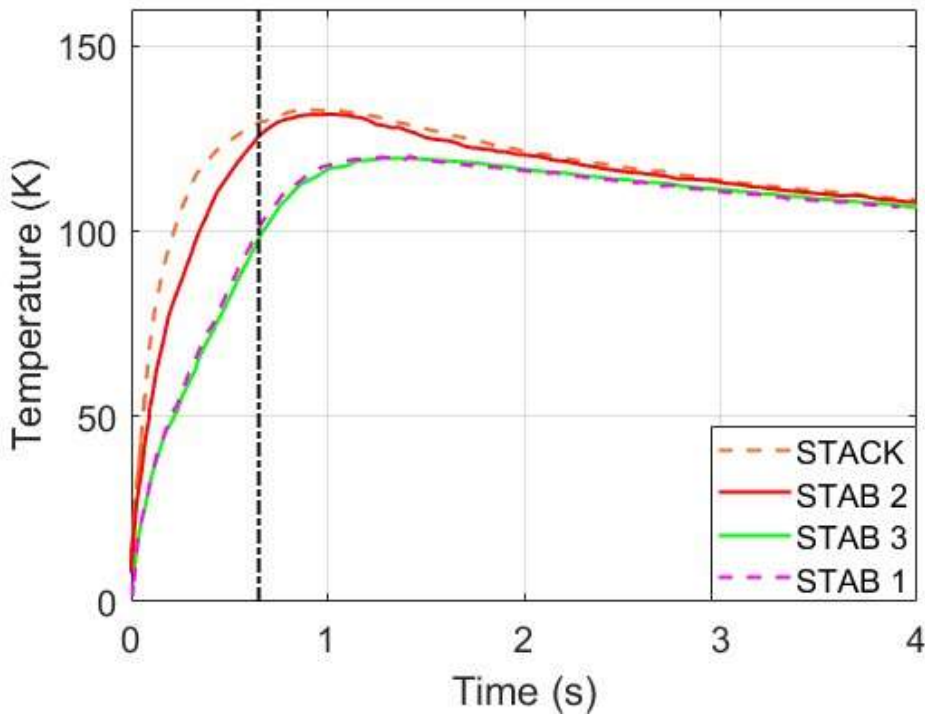

Figure 3.4 – 3: Results of the temperature peaks from the case study. The vertical dashed black line represents the current damping set at t=0.65 s.

The heat is deposited on the Stack, and this should initially cause a sharp increase in its temperature, in 4C but also in OpenSC^2. The thermal energy will then distribute by conduction both along the length of the Stack itself and transversely within the cable section, increasing the temperatures of the other components and the coolant fluid. As seen, the rise in temperatures will cause an increase in the electrical resistance of the Stack, primarily due to the variation in the critical current (temperature-dependent), which affects the change in the electrical resistivity of the SC (see Equation 2.3 – 18). This will lead to a redistribution of the current through the other components, and the flow of current, in general, will cause a continuous rise in temperature until the dumping occurs at time t = 0.65 s. At that point, the gradual reduction in current should decrease the thermal load on the cable derived from Joule heating. This should be coupled with the cooling effect of the SHe, which will eventually be able to cool the cable and its components again. What is expected to be observed is a peak in temperature across the components, and once the current discharge begins, the temperatures of the components will gradually couple together and cool down.

In Figure 3.4 – 4 the benchmark of the outcomes from OpenSC^2 against the 4C code is shown: the comparison of temperature time evolutions of the current carrier components is shown in dedicated subfigure to improve the quality of the representation.

From what we can see, expectations are being met, and the evolution of temperatures appears to reflect what was predicted.
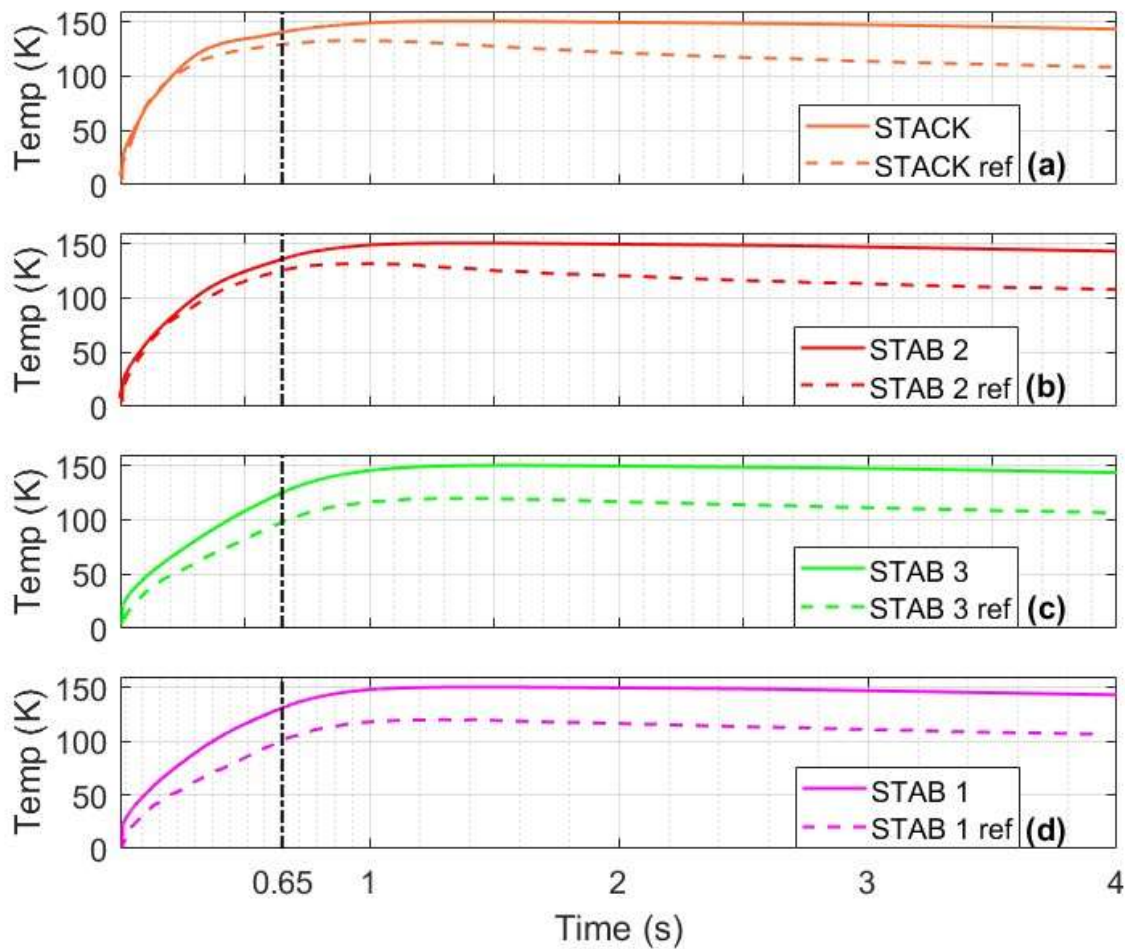
Figure 3.4 - 4: Benchmark results obtained with OpenSC². All temperatures are referenced to the midpoint of the heated zone, which has a coordinate of x = 50m.

However, there are noticeable differences in the temperature peaks, especially on the Stack. While the calculation with code 4C reached approximately 132 K, the OpenSC² computation results in about 150 K, indicating a difference of around 13%.

There are also differences visible in the other components, and overall OpenSC² records higher temperatures. These differences are certainly due to several distinctions between the two models, with the main ones being:

- Tape topology; the type of tape used in the calculation with the 4C software is not explicitly specified, and generally, the percentages of the materials could be different. Variation in the composition of the tape can have significant effects on the electrical and thermal properties of the Stack once homogenization is performed, thereby exerting a notable influence on temperature evolutions.

54

- AC losses; in the case study [40], it is explicitly stated that the calculation does not include the effects of AC losses due to the inductive effects of rapid current discharge. However, in the calculation performed with OpenSC^2, these effects are considered, as evident in Equation 2.3 – 12. By accounting for inductive effects due to discharge, higher temperatures can certainly be observed.

- Fluid properties; The properties of the fluid, although not explicitly represented in this study, are nevertheless crucial for evaluating temperature evolution. In 4C, these properties are assessed using experimental tables [51], [52], whereas in OpenSC^2, they are computed using CoolProp functions. This difference in property calculation methods could lead to variations in the computed properties.

- The spatial grid; in [40], reference is made to an adaptive mesh in space that, during the propagation of the quench front, can add nodes to the cavity, thereby increasing the precision with which spatial derivatives are computed. This tool enhances the accuracy of the calculation. Currently, OpenSC^2 lacks this capability, and the study of space convergence has shown that the maximum discretization feasible in computational terms did not ensure the highest possible calculation accuracy.

- Points in which properties are evaluated; In 4C properties are evaluated in each node, while in OpenSC^2 properties are evaluated at the midpoint (Gauss point) of the spatial discretization of the domain. These values are utilized to solve the problem's set of equations. This difference in the point where properties are computed between the two codes can lead to discrepancies in the results. For further information regarding the calculation of properties in OpenSC^2, please refer to [46].

4 Conclusions and Perspectives

The objectives of this thesis were fundamentally twofold: the first was to evaluate the coupling between the electrical and thermal models by analysing the results and verifying that the system's physics were preserved. The second objective was to benchmark a case study involving an HTS cable, which was 132 meters long and subjected to a pulsed heating of 150 J over its central 10 cm, analysing the effects of current redistribution on temperature peaks.

To be consistent as possible with the reference case [40], the study included some simplifications and reasoning for missing data.

The correctness of the system's physics with respect to the current redistribution following temperature variations during the transient was effectively verified, as the results aligned with expectations regarding current behaviour and redistribution. Indeed, the study clearly shows that an increase in the temperature of the Stack reduces its ability to transport current, and the current distribution is redistributed according to the electrical properties and geometry of the system.

Regarding temperature peaks in the case study, there are certainly marked differences, in particular OpenSC^2 calculates a temperature of 150 K against a temperature of 132 K. This difference of 13% is attributable to several factors. Firstly, the lack of information about the tape used likely led to inaccuracies in the modeling of the stack. Additionally, structural differences exist between the two electrical models: notably, the lack of computation of the effects of abrupt current changes in the case study. Furthermore, the way fluid properties are evaluated differs between the two software tools, and more in general the points in which the properties are evaluated differs between the two codes. Lastly, as also evident in the convergence study, the mesh used is not fine enough to ensure accurate temperature calculations. To date, finer meshes could not be used due to their significant computational cost implications.

Although the benchmark was relatively straightforward, the code encountered several critical issues during this thesis work, and the development environment sometimes slowed down progress.

Future steps for OpenSC^2 will undoubtedly focus on improving optimization and reducing computational costs to enable the use of finer meshes for upcoming analyses. For starting, implementing an adaptive mesh in space in OpenSC^2 could enhance simulation accuracy without significantly increasing computational costs.

Efforts are already underway in this regard, with plans for a complete refactoring to maximize software efficiency. The 13% difference in temperature peaks achieved so far can be considered a promising result, and the performance of the electrical model closely matches that of the thermal model. Nonetheless, there is still considerable work to be done to enhance the software.

OpenSC^2 now stands as one of the few software solutions capable of coupling electrical and thermal models, for both LTS and HTS, leveraging its open-source nature to potentially become a crucial tool for research institutions worldwide. Providing open access to the code allows for further enhancements, additional features, material properties, and thermal exchange correlations by those with access, promising significant advancements in future benchmarks and experimental verifications.

Moving forward, the next step will be to test this coupled electrical-thermal model on an experimental case to break the bench and verify the results, aiming to further refine the code's ability to approach or exceed previously achieved outcomes.

APPENDIX

A: Input Data

In this section, all input data used for the calculation performed with OpenSC^2, whose results are presented in section 3.4, are made explicit.

In Figure A – 1 the cross-section of the cable simulated in OpenSC^2 is depicted, along with the associated dimensions and all the measurements necessary to reproduce the same geometry.
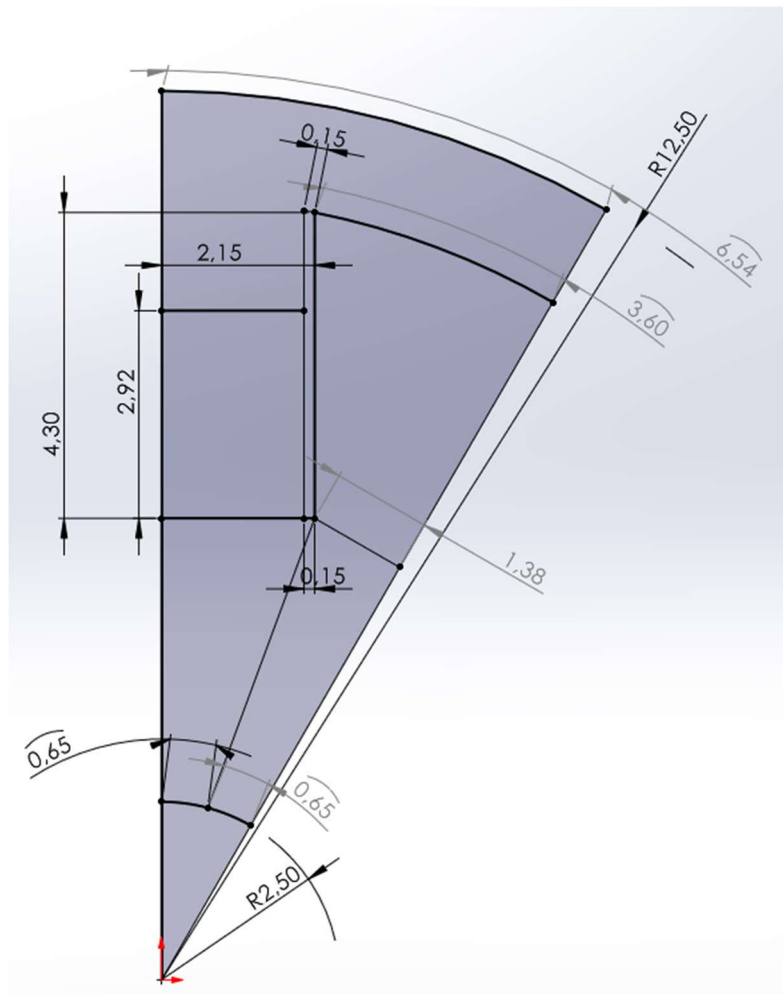

Figure A – 1: Cable cross-section with various measurements indicated in mm.

Table A – 1 contains some geometric data useful for the calculations, such as cross sections, section centroids, and the specific materials of each object into which the cable has been discretized.

Table A – 2 contains all the contact perimeters, which govern the heat exchange between the objects into which the cable is discretized. These are written in a double-entry matrix that is inherently symmetric; therefore, for the sake of brevity, the data has been transcribed for the matrix above the main diagonal.

Table A – 1: Geometric data useful for the calculations

Object	Cross Section [m]	x_barycenter [m]	y_barycenter [m]	Coolant / material
CHAN 1	$6.45 \cdot 10^{-7}$	$2.07 \cdot 10^{-3}$	$8.65 \cdot 10^{-3}$	He
CHAN 2	$1.64 \cdot 10^{-6}$	$4.30 \cdot 10^{-4}$	$1.59 \cdot 10^{-3}$	He
STACK	$5.84 \cdot 10^{-6}$	$1.00 \cdot 10^{-3}$	$7.95 \cdot 10^{-3}$	Table 3.2 – 4
STAB 1	$3.95 \cdot 10^{-6}$	$1.96 \cdot 10^{-3}$	$4.45 \cdot 10^{-3}$	Aluminum
STAB 2	$5.98 \cdot 10^{-6}$	$7.70 \cdot 10^{-4}$	$4.83 \cdot 10^{-3}$	Aluminum
STAB 3	$1.05 \cdot 10^{-5}$	$3.40 \cdot 10^{-3}$	$8.51 \cdot 10^{-3}$	Aluminum
JACKET	$1.23 \cdot 10^{-6}$	$2.50 \cdot 10^{-3}$	$1.10 \cdot 10^{-2}$	Aluminum

Table A – 2: Contact perimeter between objects

Object	CHAN 1	CHAN 2	STACK	STAB 1	STAB 2	STAB 3	JACKET
CHAN 1	0	0	2.92	0	0	4.30	1.38
CHAN 2	0	0	0	0.655	0.655	0	0
STACK	0	0	0	0	2.00	0	2.00
STAB 1	0	0	0	0	4.34	1.38	0
STAB 2	0	0	0	0	0	0	0
STAB 3	0	0	0	0	0	0	3.60
JACKET	0	0	0	0	0	0	0

B Debugging of the codes and updates

Appendix B contains all the errors and modifications made during the various simulations of the transient described in the thesis. While they are not particularly important from a scientific evidence standpoint, they encapsulate hours of work and numerous attempts to solve the problems encountered during the many tests conducted.

Furthermore, these modifications align with OpenSC[2]'s mission of being open-source software, providing a development environment where one can see what happens and, if necessary, make modifications.

B1 Grid fix

One of the early errors encountered during the initial tests of the coupled electrical and thermal model was related to the spatial mesh. This error appeared only when using a refined spatial mesh and was related to the indexing of various nodes. The leftmost initial node of the refined mesh coincided with the last node of the coarse mesh, which proved fatal in the electrical model. As described in Section 2.3.2, the code evaluates electrical resistivity during the electrical model, and subsequently multiplies it by the distance between nodes to derive coefficients for insertion into matrix R to solve the system.

Since the distance between coincident nodes is zero, the resistance was also zeroed out, rendering it impossible for the electrical model to produce a correct result.

This indexing error was not significant with the thermal model alone; hence it went unnoticed until now.

B2 The method get_electric_resistance refined

The get_electric_resistance method is implemented in the Stack and StrandMix classes, responsible for computing the equivalent electrical resistivity of the superconducting (SC) object. Throughout this thesis, this method has undergone several reformulations. This section aims to describe its original and final forms used in the latest simulations. Two pseudocodes will be presented.

```
If Ic = 0 # normal operating condition by definition
        R = R_stab
If Ic > 0
        If I_op/Ic < 0,95 # superconductive region
                R = R_sc  # from power law
        If I_op/Ic >= 0,95 # normal regim (current sharing is included)
                I_sc, I_stab = current divider(…)

                If I_stab/I_op > 0,9999 or I_sc < 1,0 # index in which all the current is
carried by the stack
                        If I_stab/I_op <= 0,9999 or I_sc >= 1,0 # in other space positions
                                R = current divider(…)
                        else # no other space positions in superconductive regime
                                R = R_stab # in all positions where I_stab/I_op > 0.9999 or
I_sc < 1.0
                else
                        # it could be in SC or in a current sharing regime
                        R = current divider(…)
```

The model, therefore, tended to ask several questions about the critical current Ic. If the latter were zero, the superconductor would be in the normal state, and thus the entire current would pass through the stabilizer, and its resistance would be the one to consider. Conversely, if in some nodes the current Ic had a value, certain threshold values would be identified, based on which the solution would be segmented, with each segment associated with a different resistance calculation, including a solution via current divider.

Written in this way, the method had many logical choices to make, some of which were based on values that tended to alter the system's physics in a very intrusive manner. Therefore, it was decided

to simplify the code, increasing readability and preserving the system's physics. The new form is written as follows:

```
If Ic < 1e-6 # normal operating condition by definition
      R = R_stab
If Ic >= 1e-6
      I_sc, I_stab = current divider(…)
      R_sc = power law(I_sc, Ic)
      R_stab = f(T) # function of the temperature
      R = parallel(R_sc, R_stab)
```

This modification, in addition to increasing code readability, has only one logical choice to make regarding the value of the critical current. If this is below a certain (very small) threshold, the entire current will be carried by the stabilizer, and thus the equivalent resistance coincides with that of the corresponding material. If the critical current exceeds a certain threshold, the equivalent resistance is calculated as seen in section 2.3.2. This preserves the physics of the system, because apart from the cutoff made on Ic, it is the current divider that assigns the currents to the SC material or the stabilizer material.

The cutoff for the critical current was set not to zero as in the previous case, but to a slightly higher value. The reason for this choice is because during the studied transient, particularly during the quench and the recovery of the temperature, very small values of Ic could be calculated in some nodes. Very small values of Ic, inserted into the non-linear equation 2.3 - 17, cause a high inaccuracy in the calculation of Isc. The Newton-Halley method has a default tolerance set to 10^{-8}. It was experimentally observed that instead of modifying the tolerance of equation 2.3 - 17 calculation each time according to the value of Ic, it was more efficient to cut off the critical current value at a sufficiently low level, to neglect the error generated.

B3 Current Sharing temperature fix

The current sharing temperature parameter was evaluated and carefully considered due to the choice of the tape, as detailed in section 3.2.3. Given the uncertainty about the specific tape used in the case study, it was crucial to ensure that the cable was initially in a superconducting state and that its operating point remained below the critical current and current sharing temperature parameters. This ensured that the initiation of the quench could be attributed solely to the thermal load applied during the transient.

During the parameter evaluation, it was observed that the operational current density considered for calculating the current sharing temperature was not the one flowing through the Stack object, but rather the total current flowing within the cable. In a transient scenario characterized by significant current redistributions (as in the case studied in this thesis), this led to calculation inaccuracies. The function was revised, and now the current density used for calculating the current sharing temperature exclusively pertains to the flow through the Stack object.

B4 The Class Stack

At the beginning of this work, the only class updated for modeling a superconducting component was the StrandMix class. The initial temperature peak evaluations were conducted using this class. However, in order to enhance calculation precision and improve alignment with the case study, it was decided to update the Stack class to accurately simulate the tape composition.

Below, the pseudocode will be presented, followed by highlighting its key step:

Initializzation of the geometric parameter # made from excel input file
Compute cross section

      thick_tot = thick_notSC + thick_SC # the thickness of notSC materials is considered separately

      A_tot = A_notSC + A_SC # also cross section contributions are split, in this way they can be used in equations 2.3 - 17

Current density cross section
      c0 physical or ingegneristic # there is a flag in input file
Properties of the stack
      Density -> Homogenization based on the material's thickness
      Thermal Conductivity -> Homogenization based on the material's thickness
      Isobaric Specific Heat -> Homogenization based on the material's thickness
      Electrical Resistivity notSC -> Homogenization based on the material's thickness

Get_electric_resistance
      Electrical Resistivity SC # see Appendix B2
      Equivalent electrical resistivity

The class homogenizes thermal and electrical properties based on the geometric parameters of the tape, which must be correctly specified by the user in the input files. Currently, up to five different materials can be added via input files, including one superconductor.

In constructing the model, we drew heavily from the StrandMix class, which performs similar homogenization operations on properties.

References

[1] M. Akhtar, "100 YEARS OF SUPERCONDUCTIVITY (1911-2011)," The Nucleus. Accessed: Jun. 26, 2024. [Online]. Available: https://www.researchgate.net/publication/232162495_100_YEARS_OF_SUPERCONDUCTIVITY_1911-2011

[2] D. Van Delft and P. Kes, "The discovery of superconductivity," *Phys Today*, vol. 63, no. 9, pp. 38–43, Sep. 2010, doi: 10.1063/1.3490499.

[3] M. Kikuchi, K. Lackner, and M. Q. Tran, "Fusion Physics," *Fusion Physics*, pp. 1–51, 2012, Accessed: Jun. 26, 2024. [Online]. Available: http://inis.iaea.org/Search/search.aspx?orig_q=RN:43116796

[4] R. Betti and O. A. Hurricane, "Inertial-confinement fusion with lasers," *Nature Physics 2016 12:5*, vol. 12, no. 5, pp. 435–448, May 2016, doi: 10.1038/nphys3736.

[5] J. Wesson and D. J. Campbell, "Tokamaks: 149 (International Series of Monographs on Physics)," p. 812, 2011, Accessed: Jun. 26, 2024. [Online]. Available: https://global.oup.com/academic/product/tokamaks-9780199592234

[6] A. H. Boozer, "What is a stellarator?," *Phys Plasmas*, vol. 5, no. 5, pp. 1647–1655, May 1998, doi: 10.1063/1.872833.

[7] N. Mitchell *et al.*, "Superconductors for fusion: a roadmap," *Supercond Sci Technol*, vol. 34, no. 10, p. 103001, Sep. 2021, doi: 10.1088/1361-6668/AC0992.

[8] A. Horvath and E. Rachlew, "Nuclear power in the 21st century: Challenges and possibilities," *Ambio*, vol. 45, no. 1, pp. 38–49, Jan. 2016, doi: 10.1007/S13280-015-0732-Y/FIGURES/6.

[9]   T. Donné, "European Research Roadmap to the Realisation of Fusion Energy," *EUROfusion*, 2018.

[10]   N. Holtkamp, "An overview of the ITER project," *Fusion Engineering and Design*, vol. 82, no. 5–14, pp. 427–434, Oct. 2007, doi: 10.1016/J.FUSENGDES.2007.03.029.

[11]   R. C. Wolf *et al.*, "Wendelstein 7-X Program - Demonstration of a Stellarator Option for Fusion Energy," *IEEE Transactions on Plasma Science*, vol. 44, no. 9, pp. 1466–1471, Sep. 2016, doi: 10.1109/TPS.2016.2564919.

[12]   L. Zani *et al.*, "Overview of Progress on the EU DEMO Reactor Magnet System Design," *IEEE Transactions on Applied Superconductivity*, vol. 26, no. 4, Jun. 2016, doi: 10.1109/TASC.2016.2536755.

[13]   C. D. Beidler *et al.*, "The Helias reactor HSR4/18," *Nuclear Fusion*, vol. 41, no. 12, p. 1759, Dec. 2001, doi: 10.1088/0029-5515/41/12/303.

[14]   M. Fujiwara *et al.*, "Overview of LHD experiments," *Nuclear Fusion*, vol. 41, no. 10, p. 1355, Oct. 2001, doi: 10.1088/0029-5515/41/10/305.

[15]   B. N. Sorbom *et al.*, "ARC: A compact, high-field, fusion nuclear science facility and demonstration power plant with demountable magnets," *Fusion Engineering and Design*, vol. 100, pp. 378–405, Nov. 2015, doi: 10.1016/J.FUSENGDES.2015.07.008.

[16]   J. Miao, L. Zhang, C. Wang, and P. Bruzzone, "Superconductivity and fusion energy—the inseparable companions," *Supercond Sci Technol*, vol. 28, no. 2, p. 024001, Dec. 2014, doi: 10.1088/0953-2048/28/2/024001.

[17]   J. E. Hirsch, "The origin of the Meissner effect in new and old superconductors," *Phys Scr*, vol. 85, no. 3, p. 035704, Feb. 2012, doi: 10.1088/0031-8949/85/03/035704.

[18]   L. Rossi, "Superconductivity: its role, its success and its setbacks in the Large Hadron Collider ofCERN," *Supercond Sci Technol*, vol. 23, no. 3, p. 034001, Feb. 2010, doi: 10.1088/0953-2048/23/3/034001.

[19] K. Seo and M. Morita, "Guidelines for LTS magnet design based on transient stability," *Cryogenics (Guildf)*, vol. 46, no. 5, pp. 354–361, May 2006, doi: 10.1016/J.CRYOGENICS.2005.11.020.

[20] A. Kawagoe *et al.*, "Winding techniques for conduction cooled LTS pulse coils for 100 kJ class UPS-SMES as a protection from momentary voltage drops," *IEEE Transactions on Applied Superconductivity*, vol. 14, no. 2, pp. 727–730, Jun. 2004, doi: 10.1109/TASC.2004.830086.

[21] D. Uglietti, "A review of commercial high temperature superconducting materials for large magnets: from wires and tapes to cables and conductors," *Supercond Sci Technol*, vol. 32, no. 5, p. 053001, Apr. 2019, doi: 10.1088/1361-6668/AB06A2.

[22] "Superconductive magnet design - Questions and Answers in MRI." Accessed: Jun. 26, 2024. [Online]. Available: https://mriquestions.com/superconductive-design.html

[23] D. C. Van Der Laan, "YBa2Cu3O7−δ coated conductor cabling for low ac-loss and high-field magnet applications*," *Supercond Sci Technol*, vol. 22, no. 6, p. 065013, Apr. 2009, doi: 10.1088/0953-2048/22/6/065013.

[24] Y. Zhang *et al.*, "Stress-Strain Relationship, Critical Strain (Stress) and Irreversible Strain (Stress) of IBAD-MOCVD-Based 2G HTS Wires under Uniaxial Tension," *IEEE Transactions on Applied Superconductivity*, vol. 26, no. 4, Jun. 2016, doi: 10.1109/TASC.2016.2515988.

[25] X. Y. Xiao, Y. Liu, J. X. Jin, C. S. Li, and F. W. Xu, "HTS Applied to Power System: Benefits and Potential Analysis for Energy Conservation and Emission Reduction," *IEEE Transactions on Applied Superconductivity*, vol. 26, no. 7, Oct. 2016, doi: 10.1109/TASC.2016.2594800.

[26] M. Takayasu, L. Chiesa, N. C. Allen, and J. V. Minervini, "Present status and recent developments of the twisted stacked-tape cable conductor," *IEEE Transactions on Applied Superconductivity*, vol. 26, no. 2, pp. 25–34, Mar. 2016, doi: 10.1109/TASC.2016.2521827.

[27] B. Shen *et al.*, "A Simplified Model of the Field Dependence for HTS Conductor on Round Core (CORC) Cables," *IEEE Transactions on Applied Superconductivity*, vol. 31, no. 8, Nov. 2021, doi: 10.1109/TASC.2021.3089117.

[28] W. Goldacker, F. Grilli, E. Pardo, A. Kario, S. I. Schlachter, and M. Vojenčiak, "Roebel cables from REBCO coated conductors: a one-century-old concept for the superconductivity of the future," *Supercond Sci Technol*, vol. 27, no. 9, p. 093001, Aug. 2014, doi: 10.1088/0953-2048/27/9/093001.

[29] L. Rossi and C. Senatore, "HTS Accelerator Magnet and Conductor Development in Europe," *Instruments 2021, Vol. 5, Page 8*, vol. 5, no. 1, p. 8, Feb. 2021, doi: 10.3390/INSTRUMENTS5010008.

[30] A. Zappatore, R. Heller, L. Savoldi, M. J. Wolf, and R. Zanino, "A new model for the analysis of quench in HTS cable-in-conduit conductors based on the twisted-stacked-tape cable concept for fusion applications," *Supercond Sci Technol*, vol. 33, no. 6, p. 065004, May 2020, doi: 10.1088/1361-6668/AB895B.

[31] C. Hu, Y. Wang, Y. Zheng, M. Li, Y. Shen, and J. Wang, "Electrothermal Analysis of Cable-in-Conduit Conductor Made from Quasi-Isotropic Strands," *IEEE Transactions on Applied Superconductivity*, vol. 33, no. 9, pp. 1–10, Dec. 2023, doi: 10.1109/TASC.2023.3329702.

[32] L. Bottura, C. Rosso, and M. Breschi, "A general model for thermal, hydraulic and electric analysis of superconducting cables," *Cryogenics (Guildf)*, vol. 40, no. 8–10, pp. 617–626, Aug. 2000, doi: 10.1016/S0011-2275(01)00019-4.

[33] "NEMO - 4C." Accessed: Jun. 26, 2024. [Online]. Available: http://www.nemo.polito.it/research/in_house_codes/4c

[34] L. Savoldi and R. Zanino, "M&M: Multi-conductor Mithrandir code for the simulation of thermal-hydraulic transients in superconducting magnets." [Online]. Available: www.elsevier.com/locate/cryogenics

[35] R. Zanino *et al.*, "Verification of the predictive capabilities of the 4C code cryogenic circuit model □ Verification of the Predictive Capabilities of the 4C Code Cryogenic Circuit Model," 2014, doi: 10.1063/1.4860896.

[36] M. Ciotti, A. Nijhuis, P. L. Ribani, L. S. Richard, and R. Zanino, "THELMA code electromagnetic model of ITER superconducting cables and application tothe ENEA stability experiment," *Supercond Sci Technol*, vol. 19, no. 10, p. 987, Aug. 2006, doi: 10.1088/0953-2048/19/10/001.

[37] "magnet system Alphysica." Accessed: Jul. 10, 2024. [Online]. Available: https://www.alphysica.com/venecia.php

[38] D. Bessette, N. Shatil, and E. Zapretilina, "Simulations of the ITER toroidal field coil operation with the VINCENTA code," *IEEE Transactions on Applied Superconductivity*, vol. 16, no. 2, pp. 795–798, Jun. 2006, doi: 10.1109/TASC.2006.873258.

[39] D. Placido and L. Savoldi, "OPENSC2/README.md at main · MAHTEP/OPENSC2 · GitHub." Accessed: Jul. 10, 2024. [Online]. Available: https://github.com/MAHTEP/OPENSC2/blob/main/README.md

[40] A. Zappatore *et al.*, "Modeling Quench Propagation in the ENEA HTS Cable-In-Conduit Conductor," *IEEE Transactions on Applied Superconductivity*, vol. 30, no. 8, Dec. 2020, doi: 10.1109/TASC.2020.3001035.

[41] "Object-Oriented Programming (OOP) in Python 3 – Real Python." Accessed: Jun. 26, 2024. [Online]. Available: https://realpython.com/python3-object-oriented-programming/

[42] L. Savoldi, D. Placido, and S. Viarengo, "Thermal-hydraulic analysis of superconducting cables for energy applications with a novel open object-oriented software: OPENSC2," *Cryogenics (Guildf)*, vol. 124, Jun. 2022, doi: 10.1016/j.cryogenics.2022.103457.

[43] S. Viarengo, F. Freschi, D. Placido, and L. Savoldi, "Current Distribution Modeling in the Open-Source OPENSC2Tool for the Multi-Physics Analysis of HTS and LTS Cables," *IEEE Transactions on Applied Superconductivity*, vol. 32, no. 6, Sep. 2022, doi: 10.1109/TASC.2022.3158309.

[44] L. Bottura, "A Numerical Model for the Simulation of Quench in the ITER Magnets," 1996.

[45] R. Zanino, I. S. De Palo, and L. Bottura, "A Two-Fluid Code for the Thermohydraulic Transient Analysis of CICC Superconducting Magnets," 1995.

[46] C. di Laurea Magistrale and R. Candidato Laura Savoldi Daniele Placido Roberto Silvestro Poccia, "POLITECNICO DI TORINO Tesi di Laurea Magistrale Object oriented modeling of LTS and HTS superconducting cables."

[47] R. Ambrosino, "DTT - Divertor Tokamak Test facility: A testbed for DEMO," *Fusion Engineering and Design*, vol. 167, p. 112330, Jun. 2021, doi: 10.1016/J.FUSENGDES.2021.112330.

[48] Y. A. Çengel, J. M. Cimbala, and A. J. (Afshin J. Ghajar, "Fundamentals of thermal-fluid sciences," p. 956.

[49] A. Augieri *et al.*, "Electrical characterization of ENEA high temperature superconducting cable," *IEEE Transactions on Applied Superconductivity*, vol. 25, no. 3, Jun. 2015, doi: 10.1109/TASC.2014.2364391.

[50] "2G HTS Wire Specification | SuperPower." Accessed: Jun. 28, 2024. [Online]. Available: https://www.superpower-inc.com/specification.aspx

[51] E. W. Lemmon, M. L. Huber, and M. O. McLinden, "NIST Standard Reference Database 23: Reference Fluid Thermodynamic and Transport Properties-REFPROP, Version 9.1." 2013. Accessed: Jul. 05, 2024. [Online]. Available: https://www.nist.gov/publications/nist-standard-reference-database-23-reference-fluid-thermodynamic-and-transport

[52] T. Kato *et al.*, "A New Wide Range Equation of State for Helium," pp. 1465–1475, 1990, doi: 10.1007/978-1-4613-0639-9_174.